Trace gas and aerosol interactions in the fully coupled model of aerosol-chemistry-climate ECHAM5-HAMMOZ:
1. Model description and insights from the spring 2001 TRACE-P experiment

L. Pozzoli,[1,2] I. Bey,[1] S. Rast,[3] M. G. Schultz,[4] P. Stier,[5,6] and J. Feichter[3]

[1] In this paper, we introduce the ECHAM5-HAMMOZ aerosol-chemistry-climate model that includes fully interactive simulations of Ox-NOx-hydrocarbons chemistry and of aerosol microphysics (including prognostic size distribution and mixing state of aerosols) implemented in the General Circulation Model ECHAM5. The photolysis rates used in the gas chemistry account for aerosol and cloud distributions and a comprehensive set of heterogeneous reactions is implemented. The model is evaluated with trace gas and aerosol observations provided by the TRACE-P aircraft experiment. Sulfate concentrations are well captured but black carbon concentrations are underestimated. The number concentrations, surface areas, and optical properties are reproduced fairly well near the surface but underestimated in the upper troposphere. CO concentrations are well reproduced in general while O_3 concentrations are overestimated by $10-20$ ppbv. We find that heterogeneous chemistry significantly influences the regional and global distributions of a number of key trace gases. Heterogeneous reactions reduce the ozone surface concentrations by $18-23\%$ over the TRACE-P region and the global annual mean O_3 burden by 7%. The annual global mean OH concentration decreases by 10% inducing a 7% increase in the global CO burden. Annual global mean HNO_3 surface concentration decreases by 15% because of heterogenous reaction on mineral dust. A comparison of our results to those from previous studies suggests that the choice of uptake coefficients for a given species is the critical parameter that determines the global impact of heterogeneous chemistry on a trace gas (rather than the description of aerosol properties and distributions). A prognostic description of the size distribution and mixing state of the aerosols is important, however, to account for the effect of heterogeneous chemistry on aerosols as further discussed in the second part of this two-part series.

1. Introduction

[2] Tropospheric trace gases and aerosols interact through a number of complex processes. The size distribution and the chemical composition of aerosols determine their optical properties, which influence the photolysis rates of trace gases. The aerosol surfaces serve as sites for heterogeneous reactions that involve a number of key species such as nitrogen pentoxide (N_2O_5), nitric acid (HNO_3), nitrogen dioxide (NO_2), hydroperoxy radical (HO_2), and ozone (O_3). Trace gases, in turn, act directly as particle precursors and are involved in the chemistry of aerosol precursors, thus contributing to the aerosol composition and mixing state. For example, sulfur dioxide (SO_2) and dimethyl sulfide (DMS) are precursors of aerosol sulfate (SO_4^{2-}). Furthermore, the oxidation of hydrocarbons can lead to the production of secondary organic aerosols (SOA). Condensation of gaseous compounds on existing particles changes the mixing state and therefore the optical properties and lifetime of a particle. For example a hydrophobic black carbon or mineral dust particle becomes hydrophilic once it is coated by sulfate, and can thus be more efficiently removed by wet

[1]Laboratoire de Modélisation de la Chimie Atmosphérique, École Polytechnique Fédérale de Lausanne, Lausanne, Switzerland.
[2]Now at Atmosphere in Earth System, Max Planck Institute for Meteorology, Hamburg, Germany.
[3]Atmosphere in Earth System, Max Planck Institute for Meteorology, Hamburg, Germany.
[4]Institute of Chemistry and Dynamics of the Geosphere: Troposphere, Forschungzentrum, Jülich, Germany.
[5]Department of Environmental Science and Engineering, California Institute of Technology, Pasadena, California, USA.
[6]Now at Atmospheric, Oceanic and Planetary Physics, University of Oxford, Oxford, UK.

Table 1. Comparison Between Previous Studies of the Effects of Heterogeneous Reactions on O_3 Concentrations in Global Models and This Work

	References			
	Martin et al. [2003][a]	*Liao et al.* [2004] and *Liao and Seinfeld* [2005]	*Tie et al.* [2005]	This Work[b]
Aerosol	SU, BC, OC, SS, DU	SU, BC, OC, SS, DU	SU, BC, OC, SS, DU	SU, BC, OC, SS, DU
INT[c]	no	yes	no	yes
EXT[d]	yes	yes	yes	yes
γ_{N2O5}[e]	0.1	variable[f]	0.04	variable[f]
γ_{HO2}[e]	0.2	0.2	0.2	0.2
γ_{NO2}[e]	10^{-4}	10^{-4}		10^{-4}
γ_{NO3}[e]	10^{-3}	10^{-3}		10^{-3}
γ_{O3}[i]		10^{-5g}	$10^{-5,g}$ $1.8 \times 10^{-4} \exp(-1000/T)$[h]	10^{-5g}
γ_{SO2}[i]		0.05; 0.005[j]		0.05; 0.005[j]
γ_{SO2}[g]		0.1; 0.0003[j]		10^{-4}
γ_{NO3}[g]				0.1
γ_{HNO3}[g]		0.1	0.1	0.1
ΔO_3[k]	A	B	C	D

[a]*Martin et al.* [2003] includes heterogeneous reactions and analyzes the photochemical effect of aerosols together with heterogeneous reactions of HO_2, N_2O_5, NO_2 and NO_3.

[b]Effect of heterogeneous reactions on all aerosol particles is considered, BASE simulation compared to sensitivity simulation NOHET.

[c]Internally mixed particles.

[d]Externally mixed particles.

[e]Uptake coefficient on wet particles, defined as all the particles in the hydrophilic modes (NS, KS, AS and CS).

[f]The uptake coefficient of N_2O_5 depends on the aerosol type (see Table 5).

[g]Uptake coefficient on mineral dust particles.

[h]Uptake coefficient on organic carbon particles.

[i]Uptake coefficient on sea salt particles.

[j]For relative humidity (RH) $\geq$ 50% and RH < 50%, respectively.

[k]A indicates that the global burden of O_3 remains unchanged, but significant regional reductions in surface O_3 concentrations are found, for example from −10% to −15% over China and Yellow Sea and from −10% to −40% over India. B indicates −13% global mean surface concentration; large variations in polluted regions, e.g., −30% in the continental Asian outflow. C indicates reductions in surface concentrations from −10% to −30% in dust source region and from −5% to −15% in polluted regions, such as U.S., eastern Europe and Asia. D indicates that the largest effect on O_3 surface concentrations (−15%) is found in dust source regions; the global mean reduction at surface is −9%; O_3 tropospheric burden is reduced by 7%.

deposition [e.g., *Koch*, 2001; *Riemer et al.*, 2004; *Croft et al.*, 2005].

[3] Both trace gases and aerosols affect the climate by influencing the Earth radiative balance. Hence a better understanding of the chemistry-aerosol-climate interactions is needed to assess past and future climate changes. In this paper we examine interactions between trace gases and aerosols in the framework of a newly developed aerosol-chemistry-climate model. Despite its complexity, this type of model allows a comprehensive investigation of the coupling and feedback processes among the various components that drive the Earth's climate [*Ravishankara et al.*, 2004].

[4] A key uncertainty in quantifying the interactions between aerosols and trace gases arises from the difficulty to reproduce the complex aerosol system in terms of size distribution, chemical composition, and mixing state. These are important parameters as they determine the optical properties of aerosols, the total aerosol surface available for heterogeneous reactions, and the uptake coefficients of gas compounds. A number of modeling studies have recently investigated the aerosol−trace gas interactions (Tables 1 and 2) and quantified their impacts on the distributions of key trace gases and aerosols. While some studies focused on heterogeneous reactions on specific aerosol types, others used more complex approaches and considered the ensemble of aerosol types present in the atmosphere. So far, however, aerosols were described with a bulk approach in most of the studies.

[5] *Liao and Seinfeld* [2005], for example, assessed the effect of heterogeneous reactions occurring on mineral dust, soot, sea salt and sulfate particles and predicted a mean global decrease of 14% in O_3 burden due to heterogeneous

reactions. *Martin et al.* [2003] evaluated the sensitivity of OH, O_3, and its precursors to the photochemical effects of aerosols and to the reactive uptake of N_2O_5, HO_2, NO_2, and NO_3 on different aerosol types (including sulfate, organic and black carbon, mineral dust, and sea salt). They found no significant change in the global O_3 burden, but significant regional variations in surface O_3 concentrations due to heterogeneous reactions and to the aerosol photochemical effect (e.g., O_3 decrease by 10−15% over northeastern China and Yellow Sea and by 10−40% over India). *Tie et al.* [2005] found a decrease in surface O_3 concentration ranging from 5 to 15% because of heterogeneous reactions of N_2O_5, HO_2, O_3, CH_2O and HNO_3 on sulfate, soot and dust particles in polluted regions and ranging from 10 to 30% in dust source regions. The effect of heterogeneous reactions on dust on O_3 concentration remains largely uncertain. *Dentener et al.* [1996] examined the effects of the reactions of N_2O_5, O_3, and HO_2 on mineral dust and found very small global effect on surface O_3 concentration with a maximum decrease of 8% in dust source regions. *Bian and Zender* [2003] found a very small effect (less than 1%) on O_3 burden while *Bauer et al.* [2004] predicted a decrease in O_3 burden of 5% due to heterogeneous reactions on mineral dust. Some papers also assessed the effect of aerosols on trace gases through the modification of photolysis rates. In general this effect on surface O_3 concentrations is found to be globally small [*Bian and Zender*, 2003; *Tie et al.*, 2005], but can be significant in aerosol source regions such as eastern Asia, Europe, United States and Sahara [*Tang et al.*, 2003; *Martin et al.*, 2003]. Note that the comparison between these studies remains somewhat difficult as the representation of aerosols (e.g., bulk approach

Table 2. Comparison Between Previous Studies of the Effects of Heterogeneous Reactions on Mineral Dust on O_3 Concentrations in Global Models and This Work

	References			
	Dentener et al. [1996]	*Bian and Zender* [2003]	*Bauer et al.* [2004]	This Work[a]
Aerosol	DU	DU	DU	SU, BC, OC, SS, DU
INT[b]	no	no	no	yes
EXT[c]	yes	yes	yes	yes
γ_{N2O5}[d]	0.1[e]	10^{-3}[e]	0.003 – 0.02[e,f]	variable[g]
γ_{HO2}[d]	0.1[e]	0.1[e]		0.2
γ_{NO2}[d]		4.4×10^{-5}[e]		10^{-4}
γ_{NO3}[d]				10^{-3}
γ_{O3}[e]	5×10^{-5}	5×10^{-5}	10^{-5}	10^{-5}
γ_{SO2}[h]				0.05; 0.005[i]
γ_{SO2}[e]	0.1; 0.0003[i]			10^{-4}
γ_{NO3}[e]		0.1	0.003	0.1
γ_{HNO3}[e]	0.1	10^{-3}	0.1	0.1
ΔO_3[j]	A	B	C	D

[a]Only the effect of mineral dust particles is considered, BASE simulation compared to sensitivity simulation NOHETDU.

[b]Internally mixed particles.

[c]Externally mixed particles.

[d]Uptake coefficient on wet particles, assuming that all the particles are in the hydrophilic modes (NS, KS, AS and CS).

[e]Uptake coefficient on mineral dust particles.

[f]30% ≥ RH ≥ 70%.

[g]The uptake coefficient of N_2O_5 depends on the aerosol type (see Table 5).

[h]Uptake coefficient on sea salt particles.

[i]For relative humidity (RH) ≥ 50% and RH < 50%, respectively.

[j]A indicates in general very small effect on O_3 surface concentration; −8% yearly averaged reduction at surface in dust source regions. B indicates tropospheric burden reduction of 0.7%; small O_3 surface concentration reductions of the order of 1 ppb in the Northern Hemisphere. C indicates tropospheric burden reduction of 5%; 20% surface concentration reduction in the tropical regions. D indicates −10% surface O_3 concentration in Saharan dust outflow; global mean reduction of 2% at surface; tropospheric O_3 burden reduction of 2%.

versus size resolved and internally mixed aerosols) and trace gas uptake coefficients vary widely among those, reflecting the large uncertainties that remain for these processes (Tables 1 and 2).

[6] Other studies have examined the impact of the trace gas–aerosol interactions on aerosol distributions. For example, *Liao and Seinfeld* [2005] included the uptake of SO_2 and HNO_3 on mineral dust in a global model and predicted a global annual mean burden decrease of 36% and 7% for sulfate and nitrate, respectively. *Bauer and Koch* [2005] investigated the heterogeneous sulfate formation on dust and estimated a global annual change of −32%, 3%, and −24% for SO_2, total sulfate and externally mixed sulfate (not associated with dust), respectively. Finally, *Bell et al.* [2005] evaluated the effects of accounting for a trace gas and a sulfate aerosol simulation on O_3 and sulfate distributions, and found a small impact on annual and global scales, but larger deviations on the regional and seasonal scales with some potential implications for the intercontinental transport of pollutants and their precursors.

[7] This paper is the first of a two-part series that quantifies to what extent accounting for interactions between aerosols and trace gases modifies the regional and global distributions of both trace gases and aerosols. In this first part, we introduce the ECHAM5-HAMMOZ aerosol-chemistry-climate model, which incorporates the HAM aerosol module [*Stier et al.*, 2005] (with a prognostic representation of the size distribution and mixing state of the aerosol components sulfate, black carbon, organic carbon, sea salt, and mineral dust) as well as the MOZ module of tropospheric chemistry (J. Rast et al., Sensitivity of a chemistry climate model to changes in emissions and the driving meteorology, manuscript in preparation, 2008) in the framework of the ECHAM5 atmospheric general circulation model [*Roeckner et al.*, 2003]. We examine in detail the trace gas and aerosol interactions by simulating the Transport and Chemical Evolution over the Pacific (TRACE-P) aircraft experiment, that took place over the north western Pacific in spring 2001. This region is strongly influenced by the Asian outflow that is rich in aerosols of different origins including fossil fuel combustion and other industrial activities, biomass burning, and soil dust [*Jacob et al.*, 2003]. The TRACE-P experiment provided a wealth of data including measurements of trace gas concentrations (O_3, NO, NO_2, CO, PAN, HNO_3, hydrocarbons, H_2O_2, CH_3OOH, OH, HO_2, CH_2O, acetone, sulfur chemistry species), aerosols (size distribution, composition, optical properties) and photolysis rates (e.g., J_{O^1D} and J_{NO_2}) that are particularly well suited for our purpose.

[8] The coupled model is described in section 2, with a special focus on the aspects related to tropospheric chemistry and aerosol interactions. We compare the model results to observations provided by the TRACE-P campaign in section 3 and examine the effects of the trace gas–aerosol interactions on the chemical composition of the TRACE-P region. We quantify the global impacts of the trace gas–aerosol interactions on the distributions of gaseous key species in section 4. Section 5 provides a summary of the main results with conclusions.

2. Model Description

[9] In the following we describe the three components of the ECHAM5-HAMMOZ (version 0) coupled model (Figure 1) including the ECHAM5 general circulation model (GCM) (section 2.1), the tropospheric chemistry module MOZ (section 2.2), and the aerosol module HAM (section 2.3), as well as the coupling between the chemistry
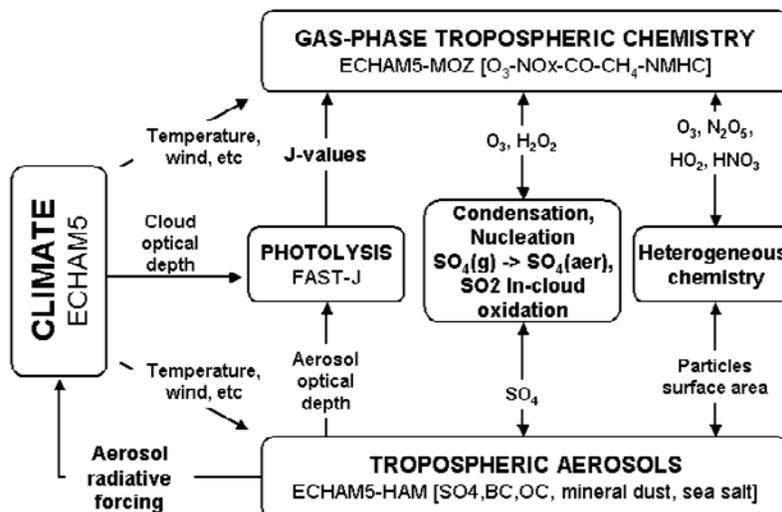
Figure 1. Schematic of the aerosol-chemistry-climate model ECHAM5-HAMMOZ.

and the aerosol modules (section 2.4). The simulation setup is described in section 2.5.

2.1. ECHAM5 General Circulation Model

[10] ECHAM5 is a GCM developed at the Max Planck Institute for Meteorology based on the numerical weather prediction model of the European Center for Medium-Range Weather Forecast (ECMWF) [*Simmons et al.*, 1989]. The prognostic variables of the model are vorticity, divergence, temperature, and surface pressure and are represented in the horizontal by truncated series of spherical harmonics. The multidimensional flux-form semi-Lagarangian transport scheme from *Lin and Rood* [1996] is used on a gaussian grid for water vapor, cloud-related variables, and chemical tracers. Stratiform clouds are described by a microphysical cloud scheme [*Lohmann and Roeckner*, 1996] with a prognostic statistical cloud cover scheme [*Tompkins*, 2002]. Cumulus convection is described by the mass flux scheme of *Tiedtke* [1989] with modifications from *Nordeng* [1994]. The radiative transfer calculation considers vertical profiles of the greenhouse gases (e.g., CO_2, O_3, CH_4), aerosols, and the cloud water and ice. The shortwave radiative transfer follows *Fouquart and Bonnel* [1980] considering 4 spectral bands, 1 for the visible-UV range (0.25–0.69 μm) and 3 for the IR (0.69–4 μm). For this part of the spectrum, cloud optical properties are calculated on the basis of Mie calculations using idealized size distributions for both cloud droplets and ice crystals [*Rockel et al.*, 1991]. The longwave radiative transfer scheme follows *Mlawer et al.* [1997] and *Morcrette et al.* [1998] and considers 16 spectral bands from 10 cm^{-1} to 3000 cm^{-1}. The cloud optical properties in the longwave spectrum are parameterized as a function of the effective radius [*Roeckner et al.*, 2003; *Ebert and Curry*, 1992].

2.2. Tropospheric Chemistry Module MOZ

[11] The MOZ chemical scheme is identical to the one used in the MOZART-2 model [*Horowitz et al.*, 2003], and includes 63 tracers and 168 reactions to represent the Ox-NOx-hydrocarbons chemistry. In this version the O^1D quenching reaction rates ($O^1D + H_2$; $O^1D + N_2$; $O^1D +$ H_2O) were updated following *Sander et al.* [2003]. Reactions involving isoprene nitrates were changed following *Fiore et al.* [2005]. Isoprene nitrates produced from the reaction of NO with the isoprene-derived peroxy radicals now correspond to a NOx sink as they are converted directly to HNO_3. Sulfur chemistry was added to the trace gas chemistry for the completion of the coupling between aerosol and chemistry simulations (see further details in section 2.4.2). Dry deposition follows the scheme of *Ganzeveld and Lelieveld* [1995]. Soluble trace gases such as HNO_3 and SO_2 are subject to wet deposition. In-cloud and below cloud scavenging follows the scheme described by *Stier et al.* [2005].

[12] We used the RETRO project data set of the year 2000 (http://www.retro.enes.org/) for the surface CO, NOx, and hydrocarbon anthropogenic emissions (T. Pulles et al., The application of the emission inventory model team: Global emissions from fuel combustion in the years 1960 to 2000, submitted to Atmospheric Environment, 2007; M. Schultz et al., A global data set of anthropogenic CO, NOx, and NMVOC emissions for 1960–2000, manuscript in preparation, 2008) and biomass burning emissions [*Schultz et al.*, 2008]. A climatology of typical injection vertical profiles is used for forest and savannah fire emissions (D. Lavoué, personal communication, 2005). Aircraft NO emissions are from *Grewe et al.* [2001]. Lightning NOx emissions are parameterized following *Grewe et al.* [2002], and are proportional to the calculated flash frequency and distributed vertically using a C-shaped profile. Lightning frequency is brought to a value that results in a global emission of 3 TgN a^{-1} (Rast et al., manuscript in preparation, 2008). The biogenic VOC emissions are calculated online with the MEGAN module of *Guenther et al.* [2006]. CO biomass burning emissions in southeast Asia account for 7 Gg/month in spring, while up to 15 Gg/month were reported from *Carmichael et al.* [2003] who estimated the Asian regional emissions using the TRACE-P observations. Therefore, in our simulations the CO biomass burning emissions were doubled in southeast Asia in March 2001.

[13] Stratospheric NOx, HNO_3, and CO concentrations are supplied as 3-D monthly means from simulations of the

Table 3. Description of the Aerosol Modes With the Dimensional Size Ranges of the Number Median Radii (r) and the Components Used in HAM Together With the Acronyms Used in the Text[a]

Mode	Soluble/Mixed		Insoluble	
	Label	Component	Label	Component
Nucleation (r ≤ 0.005 μm)	NS	SU		
Aitken (0.005 < r ≤ 0.05 μm)	KS	SU, BC, OC	KI	BC, OC
Accumulation (0.05 < r ≤ 0.5 μm)	AS	SU, BC, OC, SS, DU	AI	DU
Coarse (r > 0.5 μm)	CS	SU, BC, OC, SS, DU	CI	DU

[a]SU stands for sulfate, BC stands for black carbon, OC stands for organic carbon, SS stands for sea salt and DU stands for mineral dust. NS stands for nucleation soluble mode, KS stands for Aitken soluble, AS stands for accumulation soluble, CS stands for coarse soluble, KI stands for Aitken insoluble, AI stands for accumulation insoluble and CI stands for coarse insoluble.

MOZART-3 model [*Kinnison et al.*, 2007]. Stratospheric O_3 concentrations are prescribed as monthly mean zonal climatologies derived from observations [*Logan*, 1999; *Randel et al.*, 1998]. These concentrations are fixed at the topmost two model levels (pressures of 30 hPa and above). At other model levels above the tropopause, the concentrations are relaxed toward these values with a relaxation time of 10 days following *Horowitz et al.* [2003]. The tropopause height is diagnosed as the lowest level at which the lapse rate decreases to 2°C per kilometer or less following the World Meteorological Organization definition [*World Meteorological Organization*, 1992].

2.3. Aerosol Module HAM

[14] The tropospheric aerosol module HAM [*Stier et al.*, 2005] predicts the size distribution and composition of internally and externally mixed aerosol populations. The particle size distribution is described by 7 lognormal modes, each of them characterized by three moments including median radius, number of particles, and a fixed standard deviation (1.59 for fine particles and 2.00 for coarse particles, Table 3). Four modes are considered as hydrophilic aerosols composed of sulfate (SU), organic (OC) and black carbon (BC), mineral dust (DU), and sea salts (SS): nucleation (NS) (r < 0,005 μm), Aitken (KS) (0.005 μm < r < 0.05 μm), accumulation (AS) (0.05 μm < r < 0.5 μm) and coarse (CS) (r > 0.5 μm) (where r is the number median radius). Note that only sulfate aerosols constitute the nucleation mode. Three additional modes are considered as hydrophobic aerosols composed of an internal mixture of BC and OC in the Aitken mode (KI), and of mineral dust in the accumulation (AI) and coarse (CI) modes (Table 3). The microphysical core of HAM, M7 [*Vignati et al.*, 2004], treats the aerosol dynamics and thermodynamics in the framework of the modal structure as described above. Mineral dust particles are emitted in the accumulation and coarse insoluble modes, black carbon is emitted in the Aitken insoluble mode, while 65% of primary organic matter (OC) is emitted as internally mixed aerosols in the respective soluble mode [*Mayol-Bracero et al.*, 2002]. The biogenic monoterpene emissions of *Guenther et al.* [1995] are scaled by the factor 0.15 to estimate the production of Secondary Organic Aerosol (SOA) from biogenic sources following *Dentener et al.* [2006]. This leads to a production of 19 Tg a^{-1} of organic matter although the estimate lies between 10 and 60 Tg a^{-1} according to *Kanakidou et al.*

[2005]. In the aerosol module HAM, two processes can transform hydrophobic to hydrophilic particles, (1) condensation of gaseous sulfate (H_2SO_4) on existing particles and (2) coagulation. Only the internally mixed particles are considered to be hygroscopic and equilibrium with water vapor is accounted for. A transfer procedure is applied to the mixed modes, which allow growing particles to be transferred from one mode to the adjacent larger one.

[15] Dry deposition velocities are calculated with a serial resistance approach based on *Ganzeveld and Lelieveld* [1995] and *Ganzeveld et al.* [1998, 2006]. Wet deposition is differentiated between scavenging in stratiform and convective clouds, liquid and mixed clouds. The scavenging parameters are mode-specific with lower values for hydrophobic (externally mixed) modes [see *Stier et al.*, 2005, Table 3].

[16] The anthropogenic and biomass burning aerosol emissions are based on the AEROCOM emission inventory [*Dentener et al.*, 2006] and are representative of the year 2000. SO_2 emissions include volcanoes [*Andres and Kasgnoc*, 1998; *Halmer et al.*, 2002], vegetation fires [*van der Werf et al.*, 2003], industry, fossil fuel and biofuel [*Cofala et al.*, 2005]. Except for DMS, 97.5% of all sulfuric emissions are assumed to be in the form of SO_2 and 2.5% in the form of primary sulfate particles following *Dentener et al.* [2006].

[17] The emissions of dust and sea salt are wind driven [*Tegen et al.*, 2002; *Schulz et al.*, 2004], using the ECHAM5 10m wind speed. Marine DMS emissions are based on DMS seawater concentrations of *Kettle and Andreae* [2000] and the air-sea exchange rate based on *Nightingale et al.* [2000]. Terrestrial biogenic DMS emissions follow *Pham et al.* [1995].

[18] Aerosol optical properties (single scattering albedo, extinction cross section, and asymmetry factor) were precalculated explicitly from the Mie theory [*Toon and Ackerman*, 1981] and archived in a look-up table for a wide range of aerosol size distributions and refractive indices, and for 24 solar spectral bands. At each time step of the simulation, the aerosol optical properties are extracted from the look-up table for each mode as a function of the Mie parameter ($X = 2\pi r/\lambda$, where r is the number median radius of the lognormal mode and λ is the wavelength) and of the real and imaginary part of the refractive index. For internally mixed particles, the refractive index is calculated as a volume weighted average of the refractive indices of all components present in the mode, including aerosol water [*Stier et al.*, 2005].

2.4. Coupling Between Aerosol and Tropospheric Chemistry Simulation

[19] The following paragraphs describe the implementation of the three main mechanisms by which trace gas and aerosol interact (i.e., the coupling between the chemistry and the aerosol modules).

2.4.1. Photolytic Reactions

[20] Aerosols and clouds interact with solar radiation through multiple processes of scattering and absorption, and can thus influence photolysis rates. The Fast-J.2 algorithm [Wild et al., 2000; Bian and Prather, 2002] was implemented to calculate the photolysis rates considering the cloud and aerosol distributions. Fast-J.2 considers 18 wavelength bins in the solar spectrum from 177 to 850 nm. Wavelengths less than 177 nm are attenuated above 60 km, and those above 850 nm play no relevant role in photochemistry. Seven bins are used above 291 nm as these wavelengths reach the troposphere where clouds, surface albedo, and multiple scattering are important in determining the tropospheric photolytic radiation field, whereas 11 bins are considered below 291 nm and are important for stratospheric processes. Inputs required by Fast-J.2 include the cloud and aerosol optical depths as well as the first 8 Legendre expansion terms of the scattering phase function for the different wavelength bins.

[21] In ECHAM5, the water and ice cloud optical depth $\tau_w(\lambda)$ and $\tau_i(\lambda)$ for a specific wavelength are calculated using the following parameterization [Rockel et al., 1991]:

$$\tau_w(\lambda) = a_w \cdot LWP \cdot r_e^{b_w} \tag{1}$$

$$\tau_i(\lambda) = a_i \cdot IWP \cdot r_e^{b_i} \tag{2}$$

where LWP and IWP are the liquid and ice water content, respectively, and r_e the effective radius of the cloud water droplets or ice crystals. The two parameters $a_{w,i}$ and $b_{w,i}$ result of the fitting of cloud optical depths at a specific wavelength λ as calculated with the Mie theory for a large number of water droplet and ice crystal gamma distributions characterized by different effective radii and variances. To account for the clouds in the Fast-J.2 calculation, we performed calculations based on Mie theory using the Mishchenko et al. [1999] code to repeat the fitting and to obtain the two parameters $a_{w,i}$ and $b_{w,i}$ for the specific wavelength bins used in the Fast-J.2 algorithm (see section 1 of the auxiliary material[1]). The cloud overlap is taken into account with an approximation of the max/random overlap scheme, where the cloud optical depth in each layer is weighted by the cover fraction raised to the power of 3/2 [Briegleb, 1992; Feng et al., 2004].

[22] In addition, to account for aerosols in the Fast-J.2 calculation, we extended the look-up table of the aerosol radiative properties (originally provided by the aerosol module HAM, see section 2.3) with the first 8 Legendre expansion terms of the scattering phase function for the Fast-J.2 wavelength bins.

2.4.2. Sulfur Chemistry

[23] The chemical mechanism as described in section 2.2 was modified to include sulfur chemistry of SO_2 and DMS (Table 4). The gaseous precursors of sulfate particles are sulfur dioxide (SO_2) and dimethyl sulfide (DMS). SO_2 is oxidized by OH in the gas phase to form sulfuric acid (H_2SO_4). DMS reacts with OH following an abstraction pathway leading to the formation of SO_2, and an addition pathway leading to the formation of SO_2 (75%) and methyl sulfonic acid MSA (25%) which is directly converted to H_2SO_4. DMS is also oxidized by NO_3 to form SO_2 [Feichter et al., 1996]. The H_2SO_4 concentration in the gas phase is then used by the M7 module of HAM to calculate the aerosol sulfate formation by nucleation of new particles and by condensation on all the aerosol modes [Vignati et al., 2004]. In-cloud oxidation of SO_2 and the resulting sulfate formation is also considered [Feichter et al., 1996; Stier et al., 2005] using the calculated oxidant fields of O_3 and H_2O_2.

[24] We included the heterogeneous reaction of SO_2 on sea salt aerosols and mineral dust particles into the sulfur chemistry of ECHAM5-HAMMOZ, as further described in the next section. In ECHAM5-HAMMOZ, the SO_2, DMS, and H_2SO_4 are transported as tracers and calculated explicitly in the chemical mechanism, which also provides the O_3 and H_2O_2 fields to the aerosol module for the in-cloud SO_2 oxidation at each time step.

2.4.3. Heterogeneous Chemistry

[25] As already mentioned in section 1, previous modeling studies have shown that heterogeneous chemistry can substantially alter the distribution of trace gases on the regional and global scales. Even though significant progress has been made over the last decades, the main difficulty in assessing the impact of heterogeneous reactions on tropospheric chemistry is due to the large uncertainties in the uptake coefficients γ, which represent the probability that a molecule impacting the aerosol surface undergoes reaction [Ravishankara, 1997]. Another factor of large uncertainty is introduced by the size distribution and mixing state of aerosols as further discussed in the following.

[26] The heterogeneous reactions implemented in the coupled model are listed in Table 5 together with the uptake coefficients, while Table 6 shows the aerosol modes on which the different heterogeneous reactions are considered in the coupled model. The γ were chosen on the basis of available recommendations [e.g., Jacob, 2000] or on available experimental results as further discussed in the following. The gas to particle transfer rate K (s^{-1}) is calculated for each reaction following Schwartz [1986]:

$$K = A \left(\frac{r_e}{D_g} + \frac{4}{\nu\gamma} \right)^{-1} \tag{3}$$

where A ($cm^2 \ cm^{-3}$) is the total surface area of aerosols, r_e (cm) the effective radius (calculated as the ratio between the total volume and the surface of the aerosol mode) of the aerosol particle distribution, D_g ($cm^2 \ s^{-1}$) the gas phase molecular diffusion coefficient, ν ($cm \ s^{-1}$) is the mean molecular speed, and γ the uptake coefficient. D_g and ν can

Table 4. Chemical Reactions for the Sulfur Chemistry[a]

	Reaction Rates
Gas phase	
$SO_2 + OH \rightarrow H_2SO_4$	$k = \left(\dfrac{k_0 M}{1 + \frac{k_0 M}{k_\infty}}\right) 0.6^{\left\{1 + \left[\log\left(\frac{k_0 M}{k_\infty}\right)\right]^2\right\}^{-1}}$; $k_0 = 3 \times 10^{-31}(T/300)^{-3.3}$; $k_\infty = 1.5 \times 10^{-12}$
$DMS + OH \rightarrow SO_2$[b]	$k = 1.2 \times 10^{-11} \exp(-260/T)$
$DMS + OH \rightarrow 0.75\ SO_2 + 0.25\ H_2SO_4$[c]	$k = \dfrac{T \exp(-234/T) + 8.46 \times 10^{-10} \exp(7230/T) + 2.68 \times 10^{-10} \exp(7810/T)}{1.04 \times 10^{11} T + 88.1 \exp(7460/T)}$
$DMS + NO_3 \rightarrow SO_2$	$k = 1.9 \times 10^{-13} \exp(500/T)$
Aqueous phase	
$SO_2 \rightleftharpoons S(IV)$	$k = 1.36 \exp(4250/T)$
$H_2SO_4 \rightleftharpoons S(VI)$	$k = 1.2 \times 10^{-2} \exp(2010/T)$
$O_3(gas) \rightleftharpoons O_3(liq)$	$k = 1.03 \times 10^2 \exp(2830/T)$
$H_2O_2(gas) \rightleftharpoons H_2O_2(liq)$	$k = 7.73 \times 10^4 \exp(-7310/T)$
$S(IV) + H_2O_2(liq) \rightarrow SO_4^{2-}(aer)$	$\dfrac{d[S(IV)]}{dt} = \dfrac{k[H_2O_2][SO_2]}{0.1 + [H^+]}$; $k = 8 \times 10^4 \exp\left[-3650\left(\frac{1}{T} - \frac{1}{298}\right)\right]$
$S(IV) + O_3(liq) \rightarrow SO_4^{2-}(aer)$	$\dfrac{d[S(IV)]}{dt} = \left(k_1 + \frac{k_2}{[H^+]}\right)[O_3][S(IV)]$; $k_1 = 4.39 \times 10^{11} \exp(-4131/T)$; $k_2 = 2.56 \times 10^3 \exp(-926/T)$
Heterogeneous reactions	
$SO_2 + \text{Sea Salt} \rightleftharpoons SO_4^{2-}(aer)$	see Table 5 and section 2.4.3
$SO_2 + \text{Mineral Dust} \rightleftharpoons SO_4^{2-}(aer)$	see Table 5 and section 2.4.3

[a]All the reaction rates are taken from JPL, Chemical Kinetics and Photochemical Data for Use in Atmospheric Studies [*Atkinson et al.*, 2004], except for the reactions of S(IV) with H_2O_2 and O_3, taken from *Martin et al.* [1981] and *Maahs* [1983], respectively. The reactions in the gas phase are included directly in the chemical mechanism of MOZ, while the reactions in the aqueous phase are calculated by the aerosol module HAM. The heterogeneous reactions of SO_2 on sea salt and dust particles are included in the BASE simulation.
[b]Abstraction pathway.
[c]Addition pathway.

be expressed, respectively, as [e.g., *Chapman and Cowling*, 1970; *Davis*, 1983]:

$$D_g = \frac{3}{8 N_A d_g^2 \rho_{air}} \sqrt{\frac{R T m_{air}}{2\pi}\left(\frac{m_g + m_{air}}{m_g}\right)} \qquad (4)$$

$$\nu = \sqrt{\frac{8RT}{\pi m_g}} \qquad (5)$$

where N_A is the Avogadro number, d_g (m) the diameter of the gas molecule, ρ_{air} (g m^{-3}) air density, and m_{air} and m_g (g mole^{-1}) the molecular weights of the air and of the gas, respectively.

[27] The total surface particle area for the ith aerosol mode is calculated as:

$$A_i = 4\pi r_{n,i}^2 N_i \qquad (6)$$

where N_i is the number of particles in the mode and $r_{n,i}$ is the radius of average surface of the ith mode.

[28] In the model we consider that heterogeneous reactions occur on both externally and internally mixed particles. For externally mixed particles, the gas to particle transfer is calculated following equation (3) using the effective radius and the surface of a single aerosol mode. This is the case, for instance, for the uptake of SO_2, HNO_3, O_3, and NO_3 on the accumulation and coarse insoluble modes that are composed solely by mineral dust. For internally mixed aerosols, we have to calculate an effective gas to particle transfer rate, as these particles are composed of several components that present different uptake coefficients for a given gas. For example, the reaction of N_2O_5 on sulfate can occur on all the aerosols that include sulfate, i.e., NS, KS, AS, and CS (Table 3). However only a fraction of the surface area A_i of the ith aerosol mode (i.e., the fraction that corresponds to sulfate) is involved in the reaction of N_2O_5. Given that only little information is available in the literature about the uptake coefficients on

Table 5. Heterogeneous Reactions and Uptake Coefficients Used in This Work

Reactions	Aerosol	Uptake Coefficients γ	References
$N_2O_5 \rightarrow 2HNO_3$	sulfate	γ_{N2O5}[a]	*Kane et al.* [2001], *Hallquist et al.* [2003]
$N_2O_5 \rightarrow 2HNO_3$	organic carbon	0.03 (RH $\geq$ 50%); $5.2 \times 10^{-4} \times$ RH (RH < 50%)	*Thornton et al.* [2003]
$N_2O_5 \rightarrow 2HNO_3$	black carbon	0.005	*Sander et al.* [2003]
$N_2O_5 \rightarrow 2HNO_3$	sea salt	0.03 (RH $\geq$ 50%); 0.005 (RH < 50%)	*Atkinson et al.* [2004]
$N_2O_5 \rightarrow 2HNO_3$	mineral dust	$0.003 - 0.02$ (30% $\leq$ RH $\leq$ 70%)	*Bauer et al.* [2004]
$NO_3 \rightarrow HNO_3$	wet aerosols[b]	0.001	*Jacob* [2000]
$NO_2 \rightarrow 0.5HNO_3 + 0.5HNO_2$	wet aerosols[b]	0.0001	*Jacob* [2000]
$HO_2 \rightarrow 0.5H_2O_2$	wet aerosols[b]	0.2	*Jacob* [2000]
$SO_2 \rightarrow SO_4^{2-}(aer)$	sea salt	0.05 (RH $\geq$ 50%); 0.005(RH < 50)	*Song and Carmichael* [2001]
$SO_2 \rightarrow SO_4^{2-}(aer)$	mineral dust	10^{-4}	*Ullerstam et al.* [2002, 2003]
$HNO_3 \rightarrow NO_3^-(aer)$	mineral dust	0.1	*Bauer et al.* [2004]
$NO_3 \rightarrow NO_3^-(aer)$	mineral dust	0.1	*Bian and Zender* [2003]
$O_3 \rightarrow$ products	mineral dust	10^{-5}	*Bauer et al.* [2004]

[a]$\gamma_{N2O5} = 10^{\beta(T)} \times (2.79 \times 10^{-4} + 1.3 \times 10^{-4} \times RH - 3.43 \times 10^{-6} \times RH^2 + 7.52 \times 10^{-8} \times RH^3)$; $\beta(T) = -4 \times 10^{-2} \times (T - 294)$ for T $\geq$ 282 K; $\beta(T) = 0.48$ for T < 282 K.
[b]Wet particles are defined as all the particles in the hydrophilic/soluble modes of HAM (NS, KS, AS and CS).

Table 6. Aerosol Modes on Which the Heterogeneous Reactions Take Place in ECHAM5-HAMMOZ[a]

Trace Gases	Aerosols	Soluble				Insoluble		
		NS	KS	AS	CS	KI	AI	CI
	SU	VW	VW	VW	VW			
	BC		VW	VW	VW	VW		
N_2O_5	OC		VW	VW	VW	VW		
	SS			VW	VW			
	DU			VW	VW		ES	ES
NO_3	WET[b]	ES	ES	ES	ES			
HO_2	WET[b]	ES	ES	ES	ES			
NO_2	WET[b]	ES	ES	ES	ES			
SO_2	SS			VW	VW			
SO_2	DU			VW	VW		ES	ES
HNO_3	DU			VW	VW		ES	ES
NO_3	DU			VW	VW		ES	ES
O_3	DU			VW	VW		ES	ES

[a]"VW" corresponds to the cases for which a volume weighting of the aerosol surface is applied while "ES" means that the entire surface of the mode is considered. See Table 2 for the explanation of the labels.

[b]Wet particles are defined as all the particles in the hydrophilic/soluble modes of HAM (NS, KS, AS and CS).

internally mixed particles and that there is no direct information in the model about the surface occupied by a single component in an internally mixed aerosol particle, we choose to apply a volume weighting of the total surface area to estimate the relative contribution of each component to the surface. The gas-to-particle transfer rate K_i^x on a aerosol component x in the ith mode is thus expressed as follows:

$$K_i^x = A_i \left(\frac{r_{e,i}}{D_g} + \frac{4}{\nu \gamma_x} \right)^{-1} \frac{V_i^x}{V_i^{tot}} \qquad (7)$$

where $r_{e,i}$ is the effective radius of the ith mode, γ_x the uptake coefficient of a given molecule on the aerosol species x (SU, BC, OC, SS, DU), and V_i^x/V_i^{tot} the fraction of volume occupied by the aerosol species x in the ith mode. The effective gas-to-particle transfer rate of a given molecule on a mixed particle is then calculated as the sum of the different K_i^x. For instance, the total gas-to-particle transfer rate of N_2O_5 $K_{N_2O_5}$ is calculated as the sum of the specific $K_{N_2O_5,i}^x$ as follows:

$$K_{N_2O_5} = \sum_x^{species} \left[\sum_i^{modes} A_i \left(\frac{r_{e,i}}{D_g} + \frac{4}{\nu \gamma_x} \right)^{-1} \frac{V_i^x}{V_i^{tot}} \right] \qquad (8)$$

where x = [SU, BC, OC, SS, DU] and i = [NS, KS, AS, CS, KI, AI, CI].

[29]　We implemented the reactions of HO_2, NO_2, NO_3 on wet aerosol particles (e.g., all the soluble modes (NS, KS, AS, and CS) in the model, independently of their composition) with the uptake coefficients of 0.2, 10^{-4} and 10^{-3}, respectively, following *Jacob* [2000]. The uptake of N_2O_5 on aerosol particles follows *Evans and Jacob* [2005] and *Liao and Seinfeld* [2005], i.e., different coefficients are used for sulfate [*Kane et al.*, 2001; *Hallquist et al.*, 2003], organic carbon [*Thornton et al.*, 2003], black carbon [*Sander et al.*, 2003], sea salt [*Atkinson et al.*, 2004], and mineral dust

[*Bauer et al.*, 2004]. The O_3 uptake coefficient on mineral dust is set to 10^{-5} following *Bauer et al.* [2004].

[30]　We also considered in this work the irreversible uptake of HNO_3 on mineral dust with a $\gamma = 0.1$ as in the works by *Liao et al.* [2004], *Liao and Seinfeld* [2005], and *Bauer et al.* [2004] following the recommendation of *Hanisch and Crowley* [2001]. NO_3 uptake on mineral dust has been also reported. *Karagulian and Rossi* [2005] recommend an uptake coefficient of 0.2, *Bian and Zender* [2003] used a value of 0.1 following *Seinfeld and Pandis* [1997] and *Zhang and Carmichael* [1999], while *Bauer et al.* [2004] used a value of 3×10^{-3} following *Thomas et al.* [1998] and *Rudich et al.* [1996]. We choose to include that reaction with a $\gamma = 0.1$. One possible product of the NO_3 and HNO_3 reactions on dust is nitrate (NO_3^-), but as this compound is not included in the aerosol module HAM, these two reactions act as a sink for HNO_3 and NO_3 in our model.

[31]　For SO_2 uptake on sea salt, we use a γ of 0.05 and 0.005 for relative humidity (RH) greater or less than 50%, respectively, following *Song and Carmichael* [2001] and *Liao and Seinfeld* [2005]. The SO_2 molecules adsorbed in the sea salt particles are oxidized mainly by O_3 like in the in-cloud S(IV) oxidation. Following *Alexander et al.* [2005] and *Chameides and Stelson* [1992], we assume that the alkalinity of sea salt particles is rapidly titrated by SO2. Thus we only consider sulfate formation on fresh sea salt particles by oxidation with O_3 at a constant pH = 8 (fresh sea salt particles were diagnosed as the particles being only composed of sea salt and water). We do not take into account the sea salt alkalinity titration by HNO_3 (which can be important in tropical regions where NOx emissions dominate over SO_2 emissions [*Alexander et al.*, 2005]), and the competing aerobic S(IV) oxidation proposed by *Hoppel and Caffrey* [2005].

[32]　The SO_2 uptake coefficient on dust and the associated chemical processes are still highly uncertain. Some model studies [*Bauer and Koch*, 2005; *Liao and Seinfeld*, 2005] consider an aqueous phase oxidation of SO_2 by O_3 on mineral dust after its uptake. *Bauer and Koch* [2005] chose an uptake coefficient of 10^{-4} for RH > 60% and 10^{-7} for RH < 60% on the basis of the work of *Usher et al.* [2002, 2003] and *Ullerstam et al.* [2002, 2003]. *Dentener et al.* [1996] and *Liao and Seinfeld* [2005] used a value of 0.1 for RH > 50% and 3×10^{-4} for dryer conditions. *Usher et al.* [2002] suggested that SO_2 is irreversibly adsorbed on dust surface and that adsorbed SO_2 can be oxidized by O_3 in the gas phase. They used a Knudsen cell reactor (that allows an estimation of the uptake coefficient by measuring the loss of SO_2) and found a γ ranging from 10^{-2} to 10^{-3} on geometric surfaces of various powders, and from 10^{-4} to 10^{-5} on total internal (BET) surfaces. *Ullerstam et al.* [2002] used the DRIFT method (that allows an estimation of the reactive uptake coefficient by measuring the formation of products, e.g., sulfate) and found a γ of 10^{-3} on geometric surfaces and 10^{-6} on BET surfaces. One can assume that the reactive uptake coefficient represents a measure of both the reversible SO_2 adsorption followed by the oxidation of O_3. Furthermore, *Ullerstam et al.* [2002] measured a 47% increase in sulfate for samples exposed to a RH of 80%

Table 7. Sensitivity Simulations[a]

Labels	N_2O_5 on Wet Aerosols	NO_3 on Wet Aerosols	NO_2 on Wet Aerosols	HO_2 on Wet Aerosols	SO_2 on Sea Salt	SO_2 on Mineral Dust	HNO_3 on Mineral Dust	NO_3 on Mineral Dust	O_3 on Mineral Dust	Sulfate Formation on Sea Salt	Sulfate Formation on Dust	Mineral Dust Coating by SO_2 Uptake
BASE	yes	yes	yes	yes	yes	yes	yes	yes	yes	yes	yes	yes
NOHETDU	yes	yes	yes	yes	yes					yes		
NOHET												
NOSO4HET	yes	yes	yes	yes	yes	yes	yes	yes	yes			

[a]"Yes" means that reactions and processes were included in the specific simulation.

after a first exposure to SO_2, indicating that the previously saturated dust surface can be regenerated in wet conditions (i.e., some reaction sites can become newly available). Following these various recommendations we chose to use an uptake coefficient of 10^{-4} and assumed that all the SO_2 molecules adsorbed on dust particles produce sulfate. We account for the saturation of dust particles and considered a particle to be saturated when it is covered by a monolayer of sulfate molecules. Thus externally mixed insoluble dust particles can become soluble because of sulfate coating by SO_2 uptake and can be transferred to the corresponding soluble modes.

2.5. Model Simulation Setup

[33] We performed simulations using the coupled model ECHAM5-HAMMOZ with a spectral resolution of T42 corresponding to about 2.8×2.8 degrees in the horizontal dimension and 31 vertical σ levels from the surface up to 10 hPa, and with a 20-min time step. To reproduce the meteorological conditions of the TRACE-P experiment (spring 2001), the model was driven by the ECMWF ERA40 meteorological fields (available every 6 h). In that configuration, the prognostic variables of ECHAM5 (vorticity, divergence, temperature, and surface pressure) are relaxed toward the ERA40 reanalysis data every 3 h [*Jeuken et al.*, 1996]. Four simulations were conducted for the year 2001 (Table 7) including (1) BASE, a standard simulation that accounts for all the couplings between the chemistry and aerosol modules, with sulfur chemistry, heterogeneous reactions (including all reactions listed in Table 5), and the effect of aerosols on photolysis reactions (section 2.4); (2) NOHETDU, a simulation without heterogeneous chemistry on dust; (3) NOHET, a simulation without heterogeneous chemistry; and (4) NOSO4HET, a simulation with uptake of SO_2 on sea salt and mineral dust but without sulfate formation and therefore coating of mineral dust.

[34] We conducted a 1-year spin-up (from January to December 2000) for the BASE simulation and a 1-month spin-up starting in December 2000 for the three sensitivity simulations. For long-lived species like CO, a 1-month spin-up is not enough to reach a new equilibrium state in both hemispheres, which should be acknowledged when evaluating the global influence of heterogeneous chemistry on these species (section 4).

[35] For all these simulations the aerosol optical properties calculated by HAM were used only for diagnostics, i.e., they did not feedback on the ECHAM5 radiative transfer scheme to obtain identical meteorology. Note also that a 1-month simulation using the present configuration takes 3 h (wall-clock time) on average on the NEC-SX6 supercomputer at MPI-Met in Hamburg with 8 processors and also approximatively 3 h on 24 processors of the EPFL PLEAIDES2 linux cluster (http://pleiades.epfl.ch/).

3. Trace Gas-Aerosol Interactions in the Frame of the TRACE-P Campaign

[36] A total of 36 flights were performed during the TRACE-P campaign including 16 flights by the DC8 (up to 12 km) and 22 flights by the P3B (up to 7 km) to sample the Asian continental outflow. As reported by *Jacob et al.* [2003], the main mechanisms for export of Asian pollution

Table 8. Tropospheric O_3 Budget, Burden, and Lifetime Calculated for the BASE and All the Sensitivity Simulations (Year 2001) Compared to the Mean Values (± Standard Deviation) From a Multimodel Comparison Study (Year 2000) [*Stevenson et al.*, 2006][a]

Ozone Budget	BASE	NOHET	NOHETDU	NOSO4HET	*Stevenson et al.* [2006]
P	5201	5871	5408	5209	5110 ± 606
L	4915	5452	5112	4922	4668 ± 727
D	937	1041	960	938	1003 ± 200
S_{inf}	651	622	665	652	552 ± 168
B_{O3}	397	428	406	397	344 ± 39
τ_{O3}	24.7	24.1	24.4	24.8	22.3 ± 2.0

[a]P is chemical production, L is chemical loss, D is surface deposition, and S_{inf} is stratospheric input (S_{inf} = L + D − P), all in Tg(O_3) a^{-1}. B_{O3} is the burden (Tg(O_3)) and τ_{O3} is the lifetime (τ_{O3} = B_{O3}/(L + D)) (days).

to the Pacific are wave cyclones and the associated cold fronts and warm conveyer belts (WCBs). The convective outflow was mainly confined to southeast Asia, with convective plumes reaching the upper troposphere, subsequently carried by the westerly winds into the western Pacific region. Stratospheric intrusions were also frequently sampled during the experiment.

[37] The ECHAM5-HAMMOZ coupled model is evaluated against TRACE-P observations in section 3.1 and the impacts of the trace gas-aerosol interactions are then examined on a regional basis in section 3.2.

3.1. Evaluation of the Simulated Distributions of Trace Gas and Aerosol Distributions Over the TRACE-P Region

[38] The ECHAM5-HAMMOZ modules were already evaluated individually. The ECHAM5-HAM model was thoroughly evaluated by *Stier et al.* [2005]. A good agreement was found between simulated and observed sulfate surface concentrations. 66% and 64% of total samples agreed within a factor of 2 with the measurements over U.S. and Europe, respectively. 65% and 54% of simulated black carbon and organic carbon samples, respectively, agreed within a factor of 2 with surface measurements over U.S..The model however tends to underestimate dust concentrations (only 10% of the considered samples lied within a factor of 2 compared to an observed climatology over U.S.). A number of possible explanations for this underestimate is given by *Stier et al.* [2005]. In general, the simulated global annual mean aerosol optical depth (AOD) reproduced many patterns of a composite derived from the MODIS-MISR satellite retrievals and is in good agreement with AERONET measurements.

[39] The ECHAM5-MOZ model was also evaluated against observations by Rast et al. (manuscript in preparation, 2008), *Pozzoli* [2007] and *Auvray et al.* [2007]. It was found that CO is in general well reproduced by the model, especially in the midlatitude and tropical regions of the Northern Hemisphere, both in term of concentration and seasonality. North of 40°N, the model underestimates CO monthly mean in winter and spring by 30 ppbv, while south of 40°S the seasonality is well captured but with a systematic low bias of 10−20 ppbv. The seasonality of the monthly mean O_3 concentration is fairly well captured at different heights (800, 500 and 300 hPa), but the model systematically overestimates O_3 concentrations by 10−20 ppbv throughout the column. ECHAM5-MOZ is also in the high range in terms of global O_3 production, loss, burden and lifetime as indicated by *Stevenson et al.* [2006] who

calculated mean quantities from more than 20 global CTMs and GCMs for the year 2000. The global annual mean production, loss, and deposition of O_3 calculated by the ECHAM5-HAMMOZ BASE simulation are closer to the values reported by *Stevenson et al.* [2006] (Table 8). Ongoing work indicates that an improved representation of the upper boundary conditions and updates in the chemical mechanism greatly improve the O_3 simulation but those improvements are not yet introduced in the present simulations. We focus here our evaluation of the coupled model using the observations provided by the TRACE-P experiment.

[40] We compare our model BASE simulation to observations gathered during the flights performed over the north western Pacific between 10−40°N and 110−150°E (i.e., transit flights were not considered, see Figure S1 in the auxiliary material). In this section, we limit our discussion to the DC8 observations but a comparison to the P3B observations was also performed and lead to fairly similar conclusions about the coupled model capabilities (Figures S2−S7 in the auxiliary material, as well as Figure S8 in the auxiliary material for a summary of the model skills). The western Pacific region can be divided into two subdomains (north and south of 25°N) based on the general chemical characteristics of the continental outflow over the north western Pacific [*Jacob et al.*, 2003]. The influence of anthropogenic emissions and dust storms from the Asian continent were stronger north of 25°N, while the southernmost region was characterized by a stronger biomass burning contribution from southeast Asia. The model captures these regional patterns (Figure S9 in the auxiliary material) and in the following analysis we split the TRACE-P observations into two data sets.

[41] In Figures 2−7 we show the median vertical profiles of the observed and simulated variables binned over 100-hPa vertical intervals for the ensemble of TRACE-P DC8 observations and the correlations between the observed and simulated medians. As expected, the nudged simulation reproduces well the observed temperature, specific humidity and wind speed with correlation coefficients R greater than 0.99 and only very little mean absolute biases, 1%, 27%, and 9%, respectively (Figure 2).

[42] The model reproduces fairly well the vertical profiles of CO observed in the two regions (correlation coefficient > 0.8, Figure 3), but underestimates the observed concentrations in the boundary layer both in the northern and southern regions (mean absolute bias by 13% and 17%, respectively), which may be due to too low anthropogenic
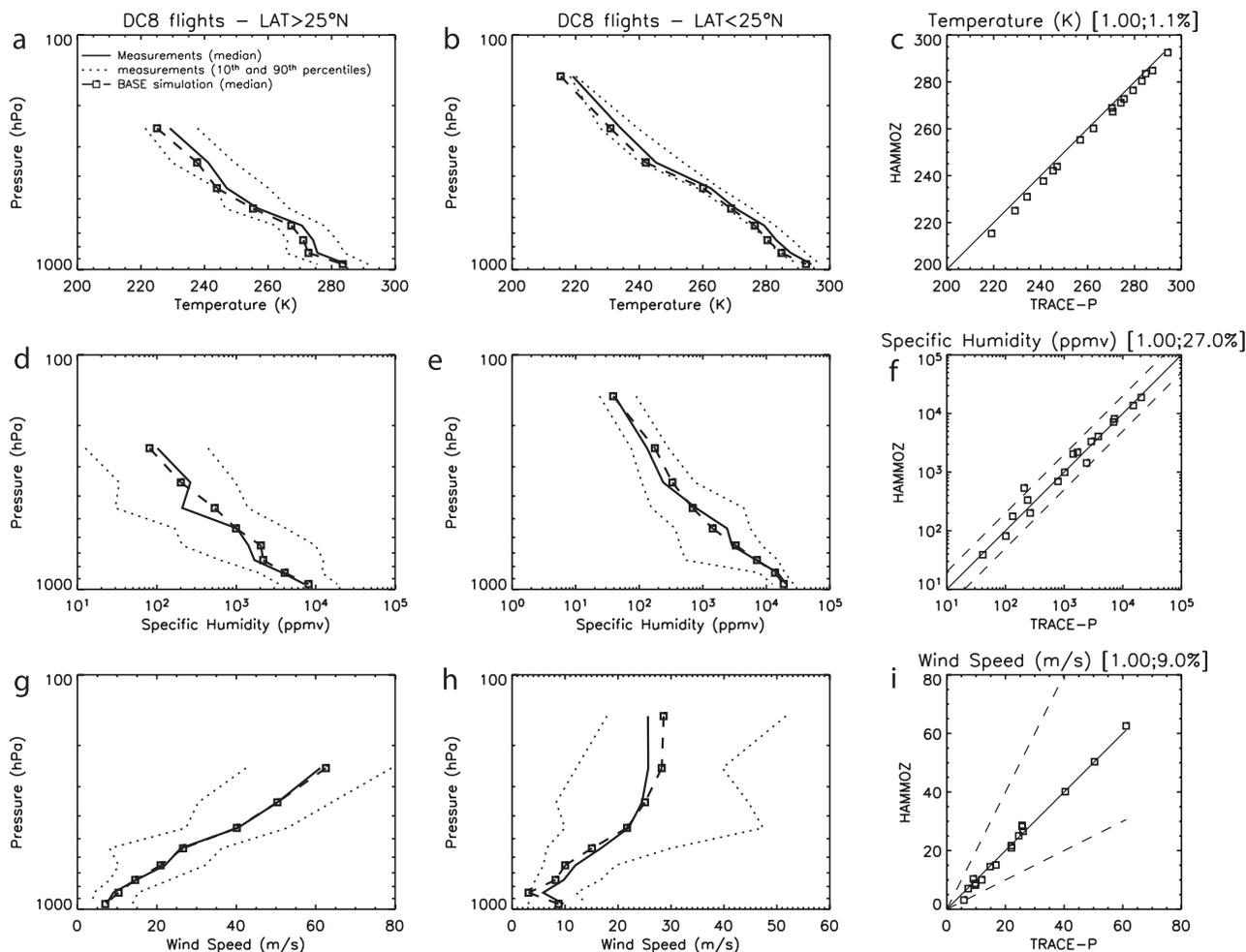
Figure 2. Vertical profiles of simulated (open square and dashed line) versus observed (solid line) medians of (a–c) temperature (K), (d–f) specific humidity (ppmv) and (g–i) wind speed (m/s) for the ensemble of TRACE-P DC8 observations (flights 6 to 17) in two different regions, latitude > 25°N (Figures 2a, 2d, and 2g) and latitude < 25°N (Figures 2b, 2e, and 2h). The model results (output every 3 h) were interpolated along the aircraft flight tracks and the data (mean averaged every 5 min) were binned in 100-hPa vertical intervals. The dotted lines represent the 10th and 90th percentiles of the observed quantities. The correlation between observed and simulated variables for the entire region (dashed lines represent the 1:2 and 2:1 ratios) is shown in Figures 2c, 2f, and 2i. The correlation coefficient and the mean absolute bias (%) are indicated in square brackets.

and biomass burning emissions in eastern Asia, as indicated also by previous evaluations of the TRACE-P campaign [e.g., *Heald et al.*, 2003; *Allen et al.*, 2004]. We find a correlation coefficient of 0.59 and 0.83 between simulated and observed NO and NO_2 concentrations, respectively. A mean absolute bias of 100% is found for NO_2, which is overestimated especially in the region below 25°N. It should be noted also that both the NO and NO_2 concentrations measured by the DC8 are significantly lower compared to those measured by the P3B over the same region, and that the comparison to the P3B observations leads to a much better agreement than with the DC8 observations with biases of 20% (see Figure S4 in the auxiliary material). As for CO, a strong latitudinal gradient is seen in SO_2 observations, with very high concentrations (more than 1 ppbv) in the northern region near the surface. The model severely overestimates concentrations measured

by both DC8 and P3B flights (by a factor greater than 2 for many samples) in the whole troposphere and for both northern and southern regions. Note that *Eisele et al.* [2003] reported a disagreement by a factor of 2 or more for NO_2 and SO_2 during an intercomparison study between DC8 and P3B flights.

[43] Simulated O_3 concentrations are systematically too high by 10 to 20 ppbv, but this appears to be a general characteristic of the model as mentioned previously. In particular, the model strongly overestimates O_3 concentrations in the boundary layer of the southern region. The observed variability in the vertical profiles of photolysis rates are well captured by the model (correlation coefficients R between observed and measured photolysis rates of J_{O^1D} and J_{NO_2} are 0.89 and 0.54, respectively, (Figure 4), and 0.93 if we remove the points between 100 and 200 hPa, where few measurements are available). The remaining
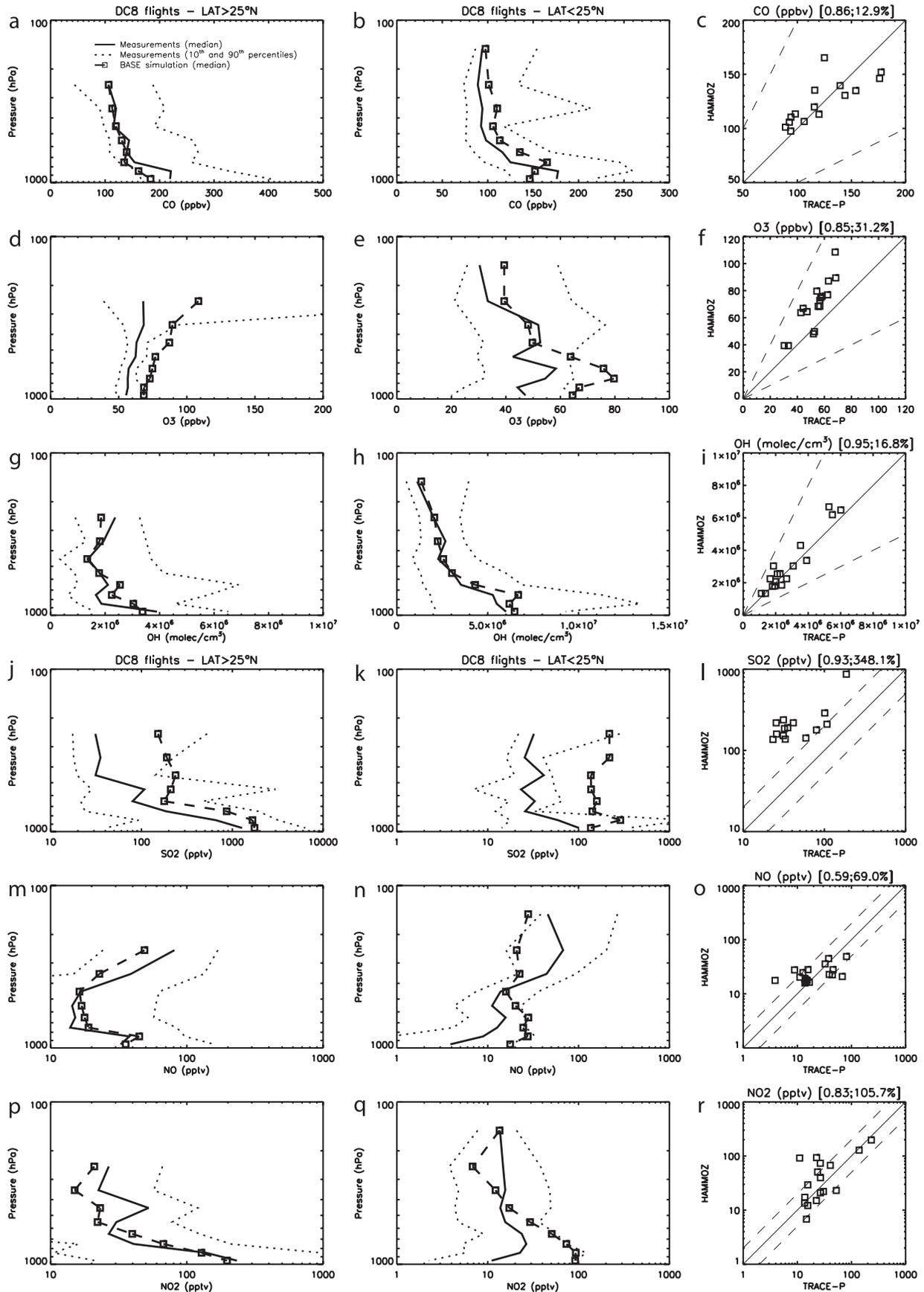
Figure 3. Same as Figure 2 for (a–c) CO (ppbv), (d–f) O_3 (ppbv), (g–i) OH (molecules/cm^3), (j–l) SO_2 (pptv), (m–o) NO (pptv) and (p–r) NO_2 (pptv).
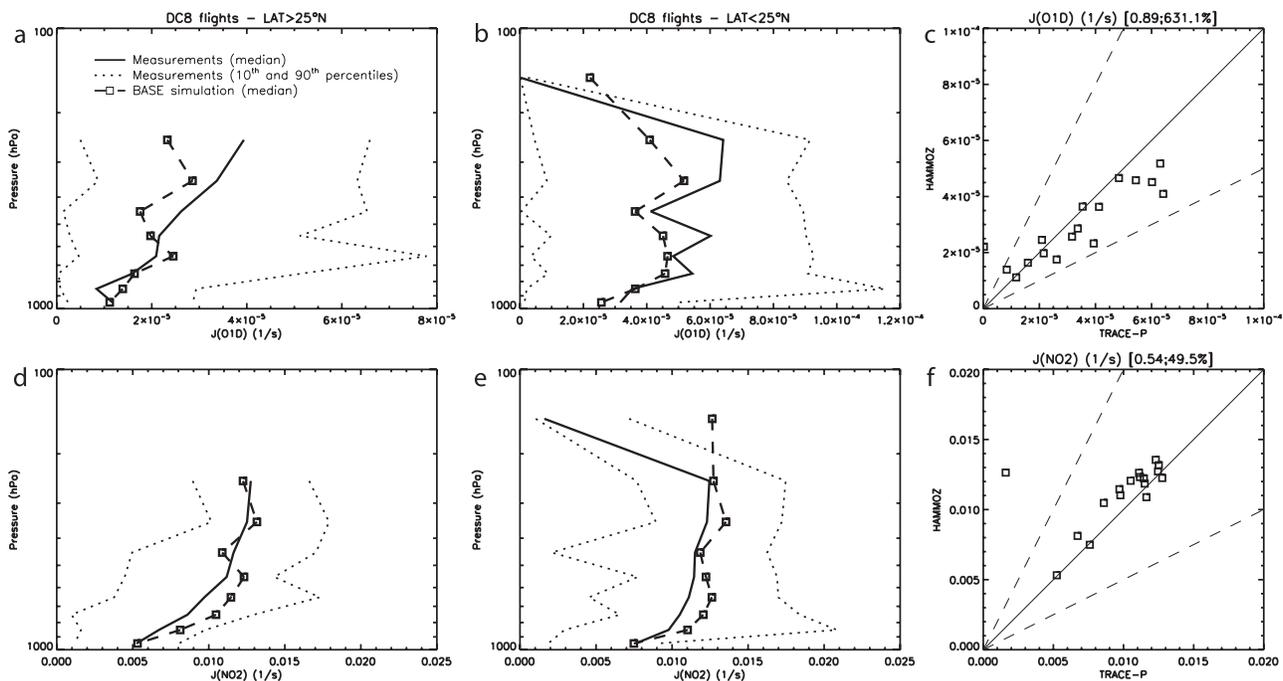
Figure 4. Same as Figure 2 for (a–c) J_{O1D} (1/s) and (d–f) J_{NO2} (1/s).

discrepancies may be due to the differences in the representation of cloud optical depths and their vertical distributions, which greatly influence the photolysis rates. *Tang et al.* [2003] conducted an analysis of the cloud and aerosol impacts on photolysis rates during the TRACE-P campaign and found that the J_{O1D} photolysis rates can vary by up to −50% below the clouds (from the surface to 1 km) and by 40% above the clouds. They also observed an increase of 6 ppbv in the O_3 concentration due to both cloud and aerosol effects on photolysis rates for a specific flight (P3B-17).

The observed OH concentrations are well reproduced (0.95 correlation coefficient and 17% mean absolute bias).

[44] Figure 5 indicates that observed sulfate concentrations are well reproduced in general (correlation coefficient of 0.91, Figure 5) although they are overestimated (mean absolute bias greater than 100%), especially in the southern region, probably because of the overestimate in SO_2 concentrations. BC concentrations were estimated from observed aerosol absorptions that were converted to mass concentrations with a mass absorption efficiency of $7 \, m^2 \, g^{-1}$

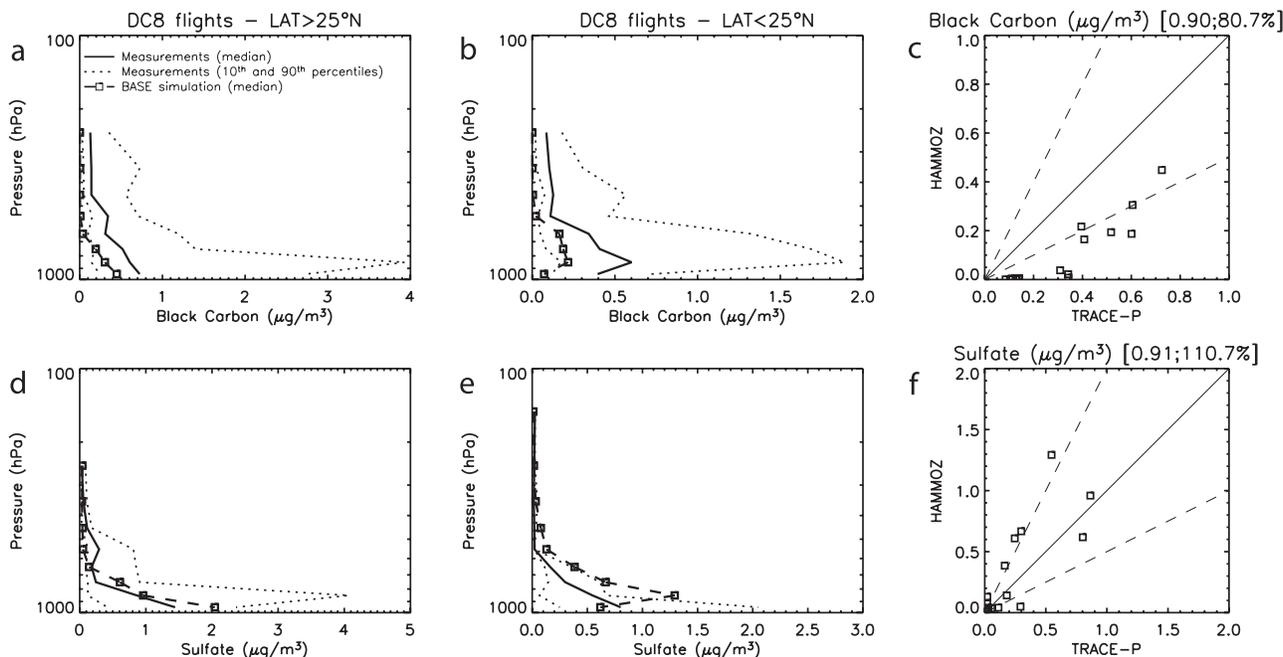**Figure 5.** Same as Figure 2 for (a–c) black carbon and (d–f) sulfate aerosol concentrations ($\mu g/m^3$).
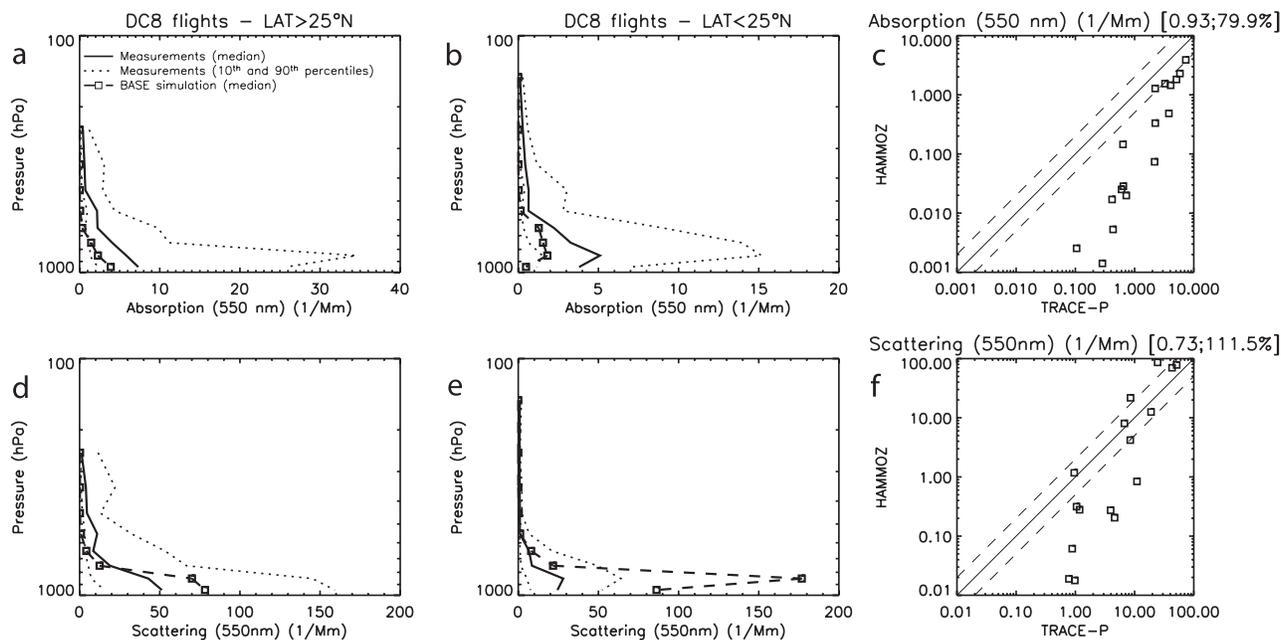
Figure 6. Same as Figure 2 for aerosol absorption at (a–c) 565 nm and (d–f) aerosol scattering at 550 nm (Mm^{-1}).

[*Clarke et al.*, 2004]. Observed BC concentrations are underestimated by 50% both in the northern and southern regions, which likely reflects too low emissions. The vertical profiles of BC concentrations, which present features similar to that of CO are relatively well captured.

[45] Comparison of the simulated aerosol optical properties to measurements performed on board of the DC8 aircraft (Figure 6) lead to similar conclusions in terms of aerosol composition, in the sense that low BC concentrations lead to a model underestimate of the aerosol absorption (at 565 nm) with a mean absolute bias of 80%. Aerosol scattering (550 nm) is relatively well reproduced in the northern region while it is greatly overestimated in the southern region, especially near the surface, with a mean absolute bias of 111%. This may be due to an overestimate of the aerosol water content in this region (Figure S9 in the auxiliary material) which increases scattering. It could also be due to an overestimate of the particle concentration number, as illustrated in Figure 7, that shows the vertical profiles of measured and observed aerosol number concentrations, aerosol particle surfaces and volumes. The quantities are measured for particles with a radius between 0.05 and 2.5 μm, therefore this range mainly covers the accumulation (0.05 < radius = 0.5 μm) and the coarse mode (radius > 0.5 μm) of HAM. The simulated number concentrations and particle surface areas are well captured by the model, even though these quantities are in general underestimated at altitudes above 600 hPa and overestimated near the surface. Note that the observations of particle number concentrations with radius ranging from 0.05 to 0.175 μm include only dry particles [*Jordan et al.*, 2003]. Hence the measured particle surface could be underestimated, in particular in the southern region that is characterized by high aerosol water contents. The model underestimate in the upper troposphere, clearly visible in Figures 7 and 8, may be due to several reasons, including (1) too strong wet

deposition rates that prevent aerosols from reaching the upper levels, (2) too low surface emissions or (3) a missing in situ source of aerosols. *Heald et al.* [2005], for instance, compared organic carbon concentrations simulated by a global chemical transport model to concentrations measured during the aircraft campaign ACE-Asia [*Huebert et al.*, 2003] (i.e., in a region similar to that sampled during the TRACE-P experiment) and found that the measured values were 10–100 times higher than the simulated concentrations even if their simulation included a parameterization for SOA formation from biogenic trace gases. They suggest that a large source of SOA is missing in the free troposphere from the oxidation of long-lived volatile organic compounds present in continental outflow.

[46] We also compared the model results to measurements acquired during single flights. We present here as an example two flights which were characterized by an enhanced aerosol loading (Figure 8) of different origins, a biomass burning outflow from southeast Asia (DC8-06) and a mineral dust episode (DC8-13). The flight DC8-06 was conducted at the beginning of the campaign to sample a variety of continental outflow patterns (Figure S10 in the auxiliary material). The aircraft crossed a front near 22°N (~0300 UTC), which extended south of a low-pressure area centered north of Korea. Both the observations and the model show a strong contrast between the clean air ahead of the front and the highly polluted air behind it (Figure 9). At 0500 (UTC) high concentrations of CO, BC, SO$_2$, and sulfate were observed and simulated near the surface, although the simulated BC and SO$_2$ concentrations are overestimated in the outflow. The DC8 then flew southwestward to sample the outflow over the South China Sea where a highly polluted layer was measured extending up to 700 hPa. Biomass burning pollution is transported (Figure S11 in the auxiliary material) and lifted up to 700 hPa by the cold front (CO concentration greater then 250 ppbv). A biomass burning convective
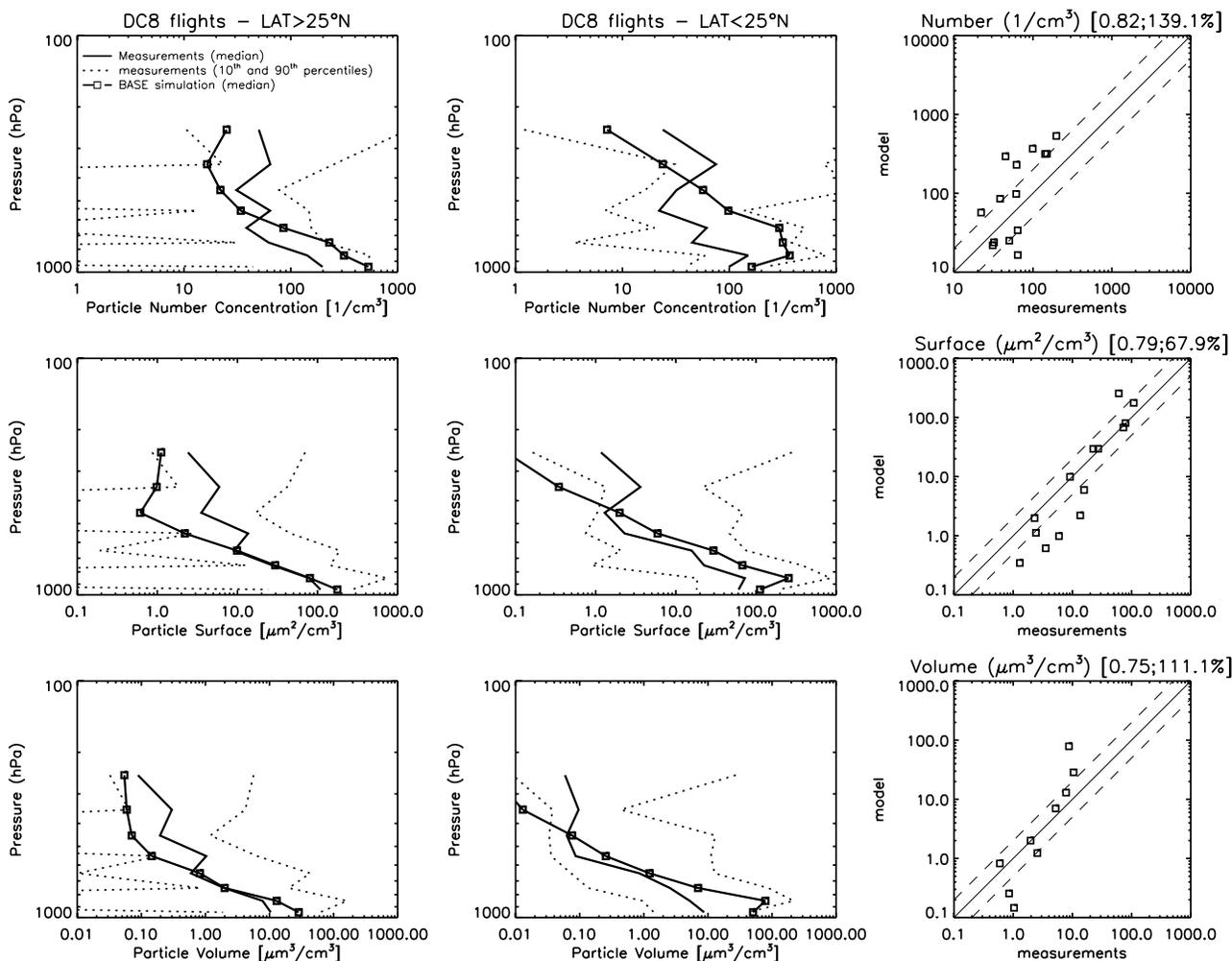
Figure 7. Same as Figure 2 for (a–c) particle number concentrations (1/cm^3), (d–f) particle surface (μm^2/cm^3) and (g–i) particle volume (μm^3/cm^3).

outflow is also visible at higher altitudes (400–600 hPa) with simulated CO concentrations up to 110 ppbv (Figure 9). Black carbon concentrations are in general clearly underestimated in the upper troposphere.

[47] The general features of the observed photolysis rates are in general well represented by the model. Some discrepancies may be attributed to the simulation of the cloud field as mentioned before. For example, the J_{O^1D} plot in Figure 9 illustrates the strong impact of clouds on the photolysis rates. Before 0400 (UTC) a thick cloud extending from 950 to 650 hPa induces a drastic reduction of the photolysis rates at the surface and, conversely, a strong increase in the upper part of the cloud and in the whole column above the cloud. Although the observed values are not as high as those simulated in the upper troposphere above the cloud, the model reproduces well most of the observed features.

[48] Flight DC8-13 (Figure S10 in the auxiliary material) was conducted to characterize the uplifting and transport of Asian pollution by a cold front and to sample convective outflow from southeast Asia in the upper troposphere, dust and pollution outflow near the coasts of China, and a stratospheric subsidence event. The meteorological condi-

tions were similar to the DC8-06 flight, with a cold front extending from a low-pressure area centered over northern Japan. After the take off from Yokota (Japan, 36°N, 139°E), a complex mixture of polluted air masses was measured, which is also well visible in the model at 0000 (UTC) with CO concentrations greater then 150 ppbv between 400 hPa and 600 hPa (Figure 10). At altitudes below 500 hPa, both measurements and model results show uplifting of fresh Asian pollution (with observed CO concentrations reaching up to 300 ppbv) associated with a pronounced frontal cloud structure (see the cloud optical depth contour lines over plotted to the J_{O1D} plot in Figure 10). The plane then crossed the cold front entering the warm side with cleaner air and thin cloud structures (0100 UTC). The flight was directed to northwest and crossed again the cold front at 26°N around 0400 (UTC) measuring once more considerable Asian pollution levels (CO up to 210 ppbv) between the surface and 600 hPa. The model reproduces these features remarkably well, both in terms of concentration and distribution of the pollutants. Just before 0500 (UTC) the flight crossed the plume of pollution coming from Shanghai at 30°N and measured some of the highest concentrations during the TRACE-P experiment (1240 ppbv
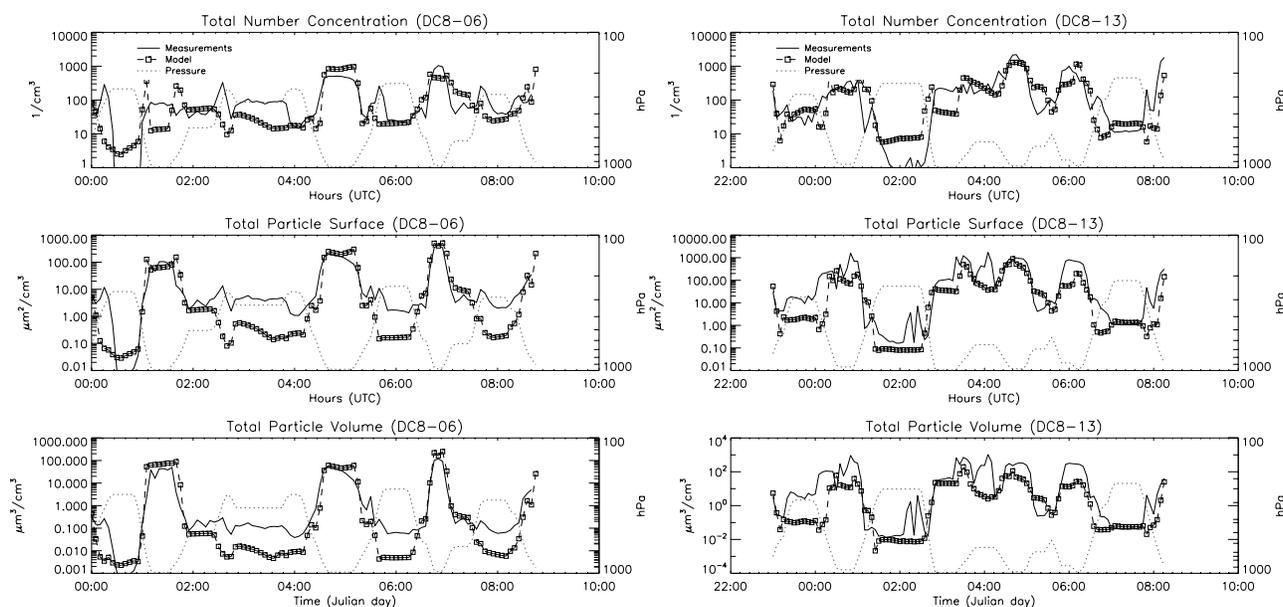
Figure 8. Observed (black line) and calculated (black dashed line and open squares) particle (0.05 > r > 1 μm) number concentrations, surfaces and volumes along the DC8-06 and DC8-13 TRACE-P flights. The dotted black lines show the pressure levels along the flight tracks (right y axis).

of CO, 140 ppbv of O_3, 2 ppbv of SO_2, and 5 μg m^{-3} of sulfate). It is clearly visible that the model captures the continental outflow between 0400 and 0700 (UTC) just in front of the Chinese coast, although it does not reproduce these high concentrations, except for SO_2. Mineral dust mixed with other pollutants were observed further north in the Yellow Sea. This is also seen in the model which produces a peak of mineral dust (60% in term of particles surface, not shown) at 0600 (UTC) mixed with sulfate ($\sim$25%) and carbonaceous aerosols (black and organic carbon, $\sim$15%) (Figure S14 (top right) in the auxiliary material).

3.2. Regional Impact of the Tropospheric Chemistry-Aerosol Coupling

[49] In the following we summarize the effects of the aerosol–trace gas interactions by analyzing the ratios between the concentrations of trace gases and aerosols calculated in the BASE simulation and those calculated in the sensitivity simulations, averaged over the TRACE-P region at three different altitudes in the troposphere.

[50] In the region north of 25°N (Table 9), the effect of heterogeneous reactions on O_3 is significant with an average reduction of 23% near the surface because of all heterogeneous reactions and of 2% because of reactions on mineral dust. OH concentrations decrease by 5% near the surface and by about 30% at higher altitudes. The contribution of mineral dust particles to this decrease is small with a maximum of 4%. HNO_3 is drastically reduced by mineral dust uptake which leads to a maximum decrease of 61% in the middle troposphere. The effect of the entire set of heterogeneous reactions is to decrease HNO_3 by up to 70%. The SO_2 concentration is not affected significantly by heterogeneous reactions on mineral dust. The maximum reduction (11%) due to the whole set of heterogeneous reactions is found in the middle troposphere.

[51] In the region south of 25°N (Table 10), the influence of the mineral dust particles is smaller. The largest effects on gases due to the heterogeneous reactions occur near the surface. A maximum reduction of 18% for O_3, 18% for OH, 45% for HNO_3, and 12% for SO_2 are seen when all heterogeneous reactions are included. Reactions on mineral dust induce maximum reductions of 3% for O_3, 4% for OH, 30% for HNO_3, and basically no reduction for SO_2. In that region we find also an increase in SO_2 concentrations in the middle and upper troposphere.

[52] Several processes contribute to the production and loss of SO_2 (section 2.4.2), including gas phase reactions, in-cloud oxidation, heterogeneous uptake on dust and sea salt particles, and the numerous interactions between gas phase and aerosols. A comparison between the BASE and the NOHETDU simulations indicates that uptake on dust has only a small effect on SO_2 (Tables 9 and 10). The direct uptake of SO_2 on sea salt occurs only on fresh particles, and thus likely contributes to the decrease of SO_2 near the surface. The increase in SO_2 at higher altitudes (725 and 500 hPa), that is seen in the region below 25°N, is more likely due to changes in trace gases (for example in OH radicals that are involved in SO_2 and DMS oxidation), and due to changes in aerosol distributions. When heterogeneous uptake of SO_2 is taken into account, the SO_2 removed by dust and sea salt is no longer available to produce H_2SO_4 and sulfate through the in-cloud oxidation and leads to direct sulfate formation. In general, the changes found in sulfate concentrations due to these heterogeneous reactions are not large, but the sulfate formation occurs through different processes with some consequences for the aerosol distribution, optical properties and lifetime. For example formation of sulfate by condensation of H_2SO_4 and the uptake of SO_2 on insoluble dust particles affect hydrophobic particles as they can become hydrophilic after sulfate coating and then can be transferred to another aerosol mode
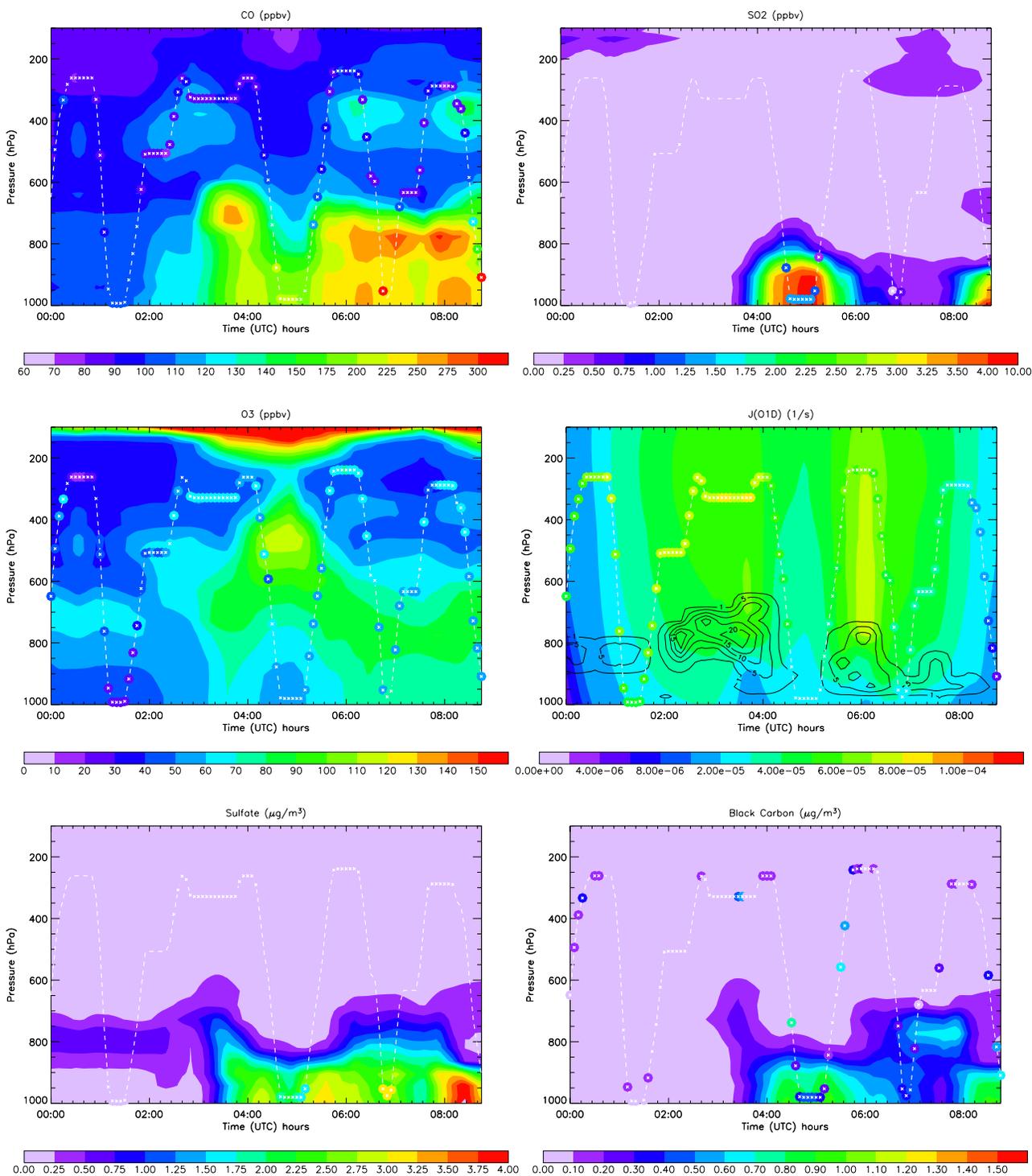
Figure 9. CO, SO_2, O_3, J_{O1D}, sulfate and black carbon vertical columns calculated by the model along the DC8-06 flight track. The colored circles represent the 5 min averaged observations. The contour lines plotted over J_{O1D} represent the cloud optical depth calculated by the model.

in the model. All these competing processes make difficult the attribution of a given variation to a single process, as shown in section 3 of the auxiliary material for a biomass burning episode (flight DC8-06) and a dust episode (flight DC8-13).

[53] As mentioned before, the changes in sulfate and SO_2 have an impact on other aerosol species. For example, in the region below 25°N, the reduction in mineral dust of 8% near the surface and 16% and 32% at higher altitudes may be due to the sulfate coating. The coating processes influence the deposition of the particles and therefore also the transport far away from the sources. We do not see a similar behavior for black carbon particles, as the study region is closer to the emission sources, namely biomass burning in the southern
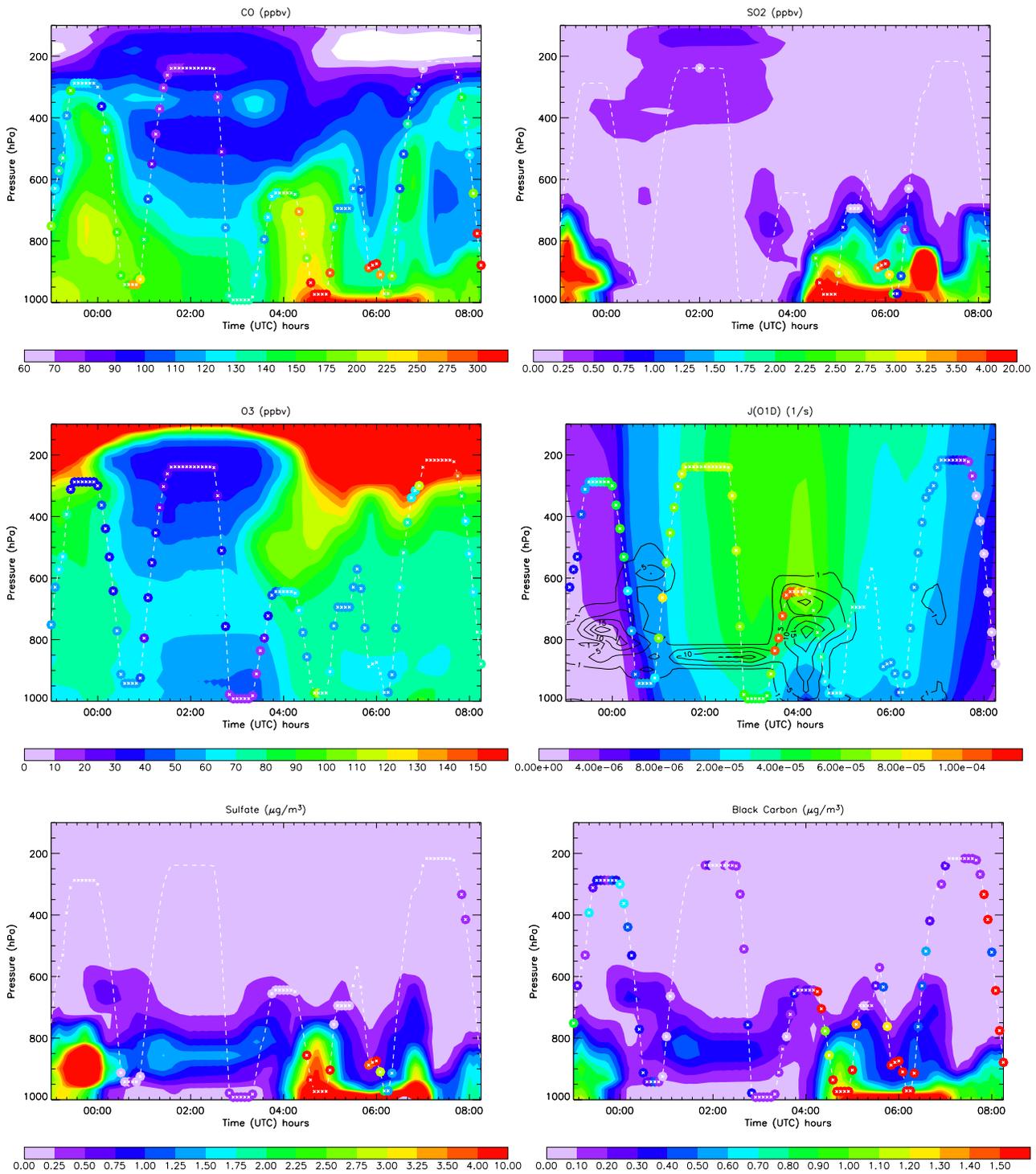
Figure 10. CO, SO$_2$, O$_3$, J$_{O1D}$, sulfate and black carbon vertical columns calculated by the model along the DC8-13 flight track. The colored circles represent the 5 min averaged observations. The contour lines plotted over J$_{O1D}$ represent the cloud optical depth calculated by the model.

Table 9. Monthly (March 2001) Mean Variations of Gases and Aerosols in the Sensitivity Simulations Over the Region Investigated by the TRACE-P Aircraft Campaign[a]

| | | Latitude > 25°N | | |
	BASE	BASE NOHETDU	BASE NOHET	BASE NOSO4HET
O_3, ppbv				
Surface	59.80	0.98	**0.77**	1.00
~725 hPa	69.62	0.97	**0.79**	1.00
~500 hPa	78.56	0.97	**0.84**	1.00
OH, molecules/cm^3				
Surface	1.05×10^6	1.00	0.95	1.00
~725 hPa	0.94×10^6	0.96	**0.67**	1.00
~500 hPa	0.66×10^6	0.96	**0.72**	1.00
HNO_3, pptv				
Surface	210.71	**0.53**	**0.51**	1.02
~725 hPa	101.95	**0.39**	**0.30**	1.06
~500 hPa	66.42	**0.44**	**0.33**	**1.15**
SO_2, pptv				
Surface	519.86	0.99	0.94	1.01
~725 hPa	497.58	0.99	**0.89**	1.01
~500 hPa	205.46	1.01	1.02	1.03
SU, $\mu g/m^3$				
Surface	0.910	1.00	1.03	1.05
~725 hPa	0.318	1.00	0.93	1.04
~500 hPa	0.034	1.00	**0.88**	1.04
BC, $\mu g/m^3$				
Surface	0.256	1.00	1.00	1.00
~725 hPa	0.088	1.00	1.01	1.00
~500 hPa	0.006	1.00	1.02	1.00
DU, $\mu g/m^3$				
Surface	3.386	0.96	0.97	0.96
~725 hPa	1.743	0.94	0.95	0.94
~500 hPa	0.132	0.91	0.91	**0.90**

[a]The region above 25°N (25−45°N; 120−155°E) is analyzed separately at three vertical levels (surface ∼1000 hPa, ∼725 hPa, ∼500 hPa). Percentage changes greater then 10% are in bold.

row). The impact of all heterogeneous reactions on aerosol particles is a reduction in surface O_3 concentrations that can reach up to 15% in the mineral dust source region, and up to 10% and 5% in the Northern and Southern Hemisphere, respectively. We find that O_3 concentrations decrease by 2% and 9% at all altitudes because of the heterogeneous reactions on mineral dust and all aerosol particles, respectively (Table 11). Globally the O_3 burden decreases by 7% (Table 12). The mineral dust particles reduce the surface O_3 concentration by 10% over the Sahara desert and in the outflow over the Atlantic Ocean, the Arabian Peninsula and over the Indian Ocean, while very small effect is seen over central Asia, Australia, and western United States.

[56] *Liao and Seinfeld* [2005] predicted a global mean decrease in surface ozone of 13.5% due to heterogeneous reactions on all aerosol particles. In the Northern Hemisphere they found larger decrease from 15% to 30% with values above 30% over the eastern United States, eastern Europe, and northern Asia, and from 5% to 10% in the Southern Hemisphere. Mineral dust particles only contribute to a global mean decrease of 4%. We predict a fairly similar distribution of the O_3 decrease due to heterogeneous reactions (see Figure 11 and Table 11), but with overall lower values. The fairly good agreement between our results and those from *Liao and Seinfeld* [2005] probably results from the use of similar uptake coefficients in the two studies (Table 1).

[57] *Martin et al.* [2003] analyzed the effects of aerosols on tropospheric oxidants through the modification of the photolysis rates and the heterogeneous reactions of NO_2, NO_3, and HO_2. They used the uptake coefficients recommended by *Jacob* [2000] for these later species as in the

region and anthropogenic (fossil fuel and megacities pollution) in the northern region. The impacts of heterogeneous reactions on aerosol distributions are discussed in details in the second part of this study [*Pozzoli et al.*, 2008].

4. Impact of the Trace Gas−Aerosol Interactions on the Global Burden of O_3 and O_3-Related Species

[54] In this section we examine the global impacts of the trace gas−aerosol interactions. We also discuss our results in light of those from previous studies that used global models (Tables 1 and 2). In general, those models include the same processes, but they differ substantially in terms of the aerosol parameterizations (resulting in varying aerosol number concentrations, size distributions, loads and spatial distributions), uptake coefficients, parameterizations of heterogeneous chemistry, etc. In particular, *Dentener et al.* [1996], *Bian and Zender* [2003], *Bauer et al.* [2004], *Martin et al.* [2003], and *Tie et al.* [2005] consider externally mixed particles while both internally and externally mixed particles are considered by *Liao et al.* [2003, 2004], and *Liao and Seinfeld* [2005]; the prognostic size distribution and mixing state of the aerosols is only described in HAM [*Stier et al.*, 2005].

[55] The annual mean surface O_3 concentrations are shown in Figure 11 (first row) together with the impact of heterogeneous reactions on mineral dust (second row) and the impact of all heterogeneous reactions on particles (third

Table 10. Same as Table 9 for the Region Below 25°N (10−25°N; 110−155°E)

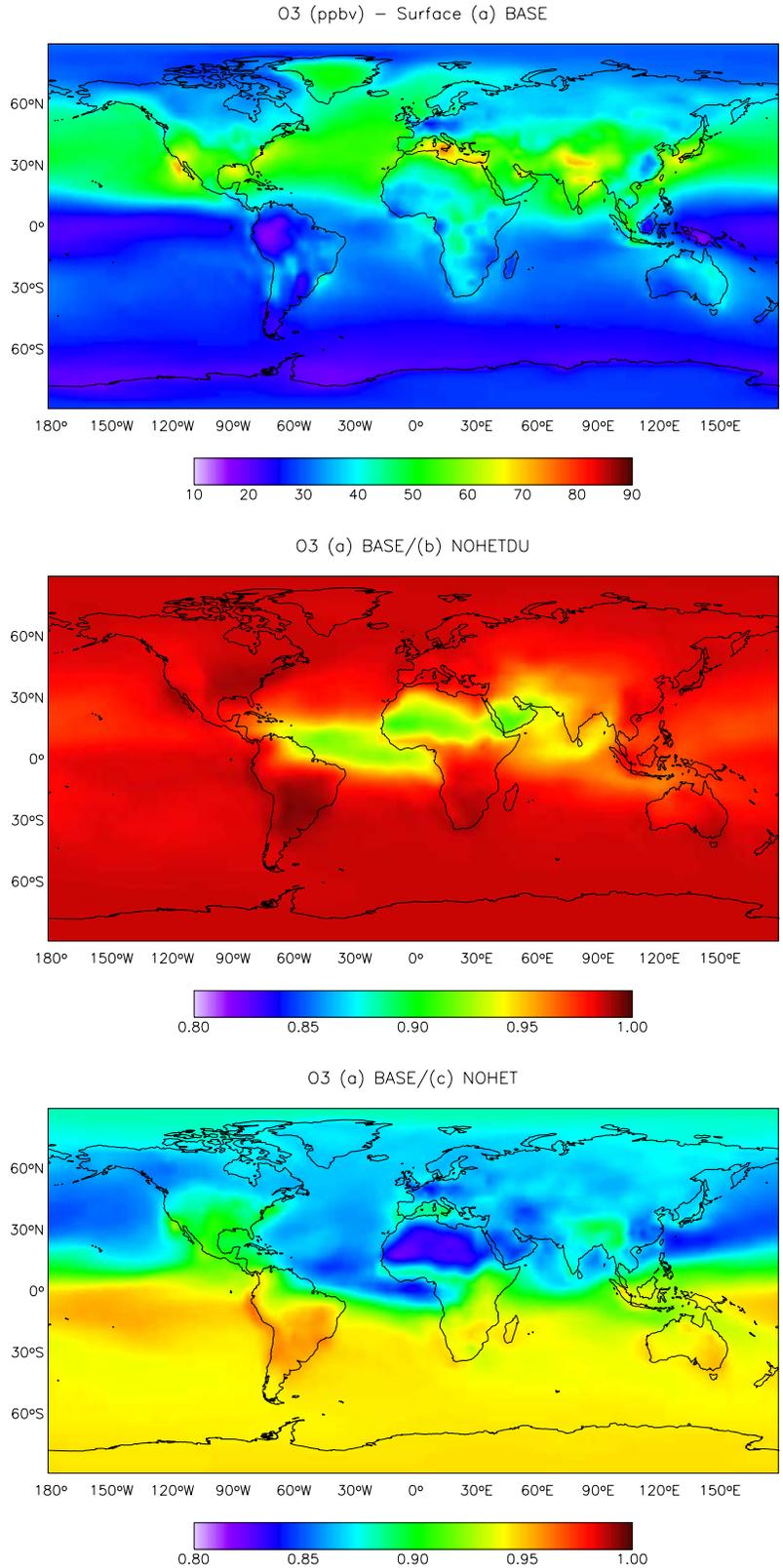| | | Latitude < 25°N | | |
	BASE	BASE NOHETDU	BASE NOHET	BASE NOSO4HET
O_3, ppbv				
Surface	52.42	0.97	**0.82**	1.00
~725 hPa	70.50	0.97	**0.90**	1.00
~500 hPa	57.18	0.98	**0.94**	1.00
OH, molecules/cm^3				
Surface	2.21×10^6	0.96	**0.82**	0.99
~725 hPa	2.23×10^6	0.96	**0.87**	1.00
~500 hPa	1.16×10^6	0.98	0.91	1.00
HNO_3, pptv				
Surface	104.51	**0.70**	**0.55**	1.03
~725 hPa	373.19	**0.63**	**0.57**	1.06
~500 hPa	102.14	**0.88**	**0.84**	1.01
SO_2, pptv				
Surface	78.17	1.00	**0.88**	**1.28**
~725 hPa	144.24	1.03	**1.10**	**1.14**
~500 hPa	151.59	1.03	1.08	**1.21**
SU, $\mu g/m^3$				
Surface	0.351	1.00	0.99	**1.16**
~725 hPa	0.408	1.00	0.97	**1.15**
~500 hPa	0.099	0.99	0.97	**1.13**
BC, $\mu g/m^3$				
Surface	0.041	1.00	1.01	1.00
~725 hPa	0.119	1.00	1.01	0.99
~500 hPa	0.005	1.00	1.01	0.95
DU, $\mu g/m^3$				
Surface	0.175	0.91	0.92	**0.90**
~725 hPa	0.113	**0.83**	**0.84**	**0.81**
~500 hPa	0.011	**0.68**	**0.68**	**0.64**

Figure 11. Annual mean O_3 surface concentration (ppbv) for the standard simulation BASE and the ratios BASE/NOHETDU and BASE/NOHET.

Table 11. Global Annual Mean Concentration Variations of Gases and Aerosols in the Sensitivity Simulations at Three Different Levels (Surface ∼1000 hPa, ∼725 hPa, and ∼500 hPa)[a]

	BASE	$\frac{BASE}{NOHETDU}$	$\frac{BASE}{NOHET}$	$\frac{BASE}{NOSO4HET}$
O_3, ppbv				
Surface	34.57	0.98	0.91	1.00
∼725 hPa	48.35	0.98	0.91	1.00
∼500 hPa	56.66	0.98	0.92	1.00
OH, molecules/cm^3				
Surface	0.75×10^6	0.98	**0.90**	1.00
∼725 hPa	0.98×10^6	0.97	**0.89**	1.00
∼500 hPa	0.80×10^6	0.97	0.91	1.00
HNO_3, pptv				
Surface	99.32	**0.85**	**0.85**	1.01
∼725 hPa	92.17	**0.78**	**0.71**	1.02
∼500 hPa	64.82	**0.83**	**0.77**	1.02
SO_2, pptv				
Surface	265.82	1.00	**0.86**	**1.16**
∼725 hPa	112.09	1.01	0.94	**1.14**
∼500 hPa	92.74	1.02	0.99	1.09

[a]Percentage changes greater then 10% are in bold.

present work. They found a large surface O_3 decrease over regions with intense emissions of both aerosols and O_3 precursors. For example, O_3 is reduced in the lower troposphere by 10–15% over northeastern China and the Yellow Sea. We find, for the same month of the year (March) and the same region, a smaller O_3 reduction (<5%) due to dust reactive uptake of trace gases, but a comparable O_3 reduction (18%) due to the full suite of heterogeneous reactions included in this work although one should note that the sensitivity simulations NOHETDU and NOHET do not include the photochemical effect of aerosols.

[58] *Tie et al.* [2005] estimated somewhat larger effects that in the present study. For example, they predicted a decrease in surface O_3 concentrations of 20% in winter (DJF) and of 15% in summer (JJA) in the Saharan dust outflow because of dust uptake of HO_2, N_2O_5, and NO and a decrease of 15% in winter and of 10% in summer over east Asia due to sulfate and soot uptake of HO_2, CH_2O, and O_3. Again we suggest this is due to differences in the heterogeneous reaction scheme. In the work of *Tie et al.* [2005], N_2O_5 and HO_2 react on both sulfate and mineral dust aerosols with a constant uptake coefficient of 0.04 and 0.2, respectively. In our model HO_2 can react with the same uptake coefficient but only on wet aerosol particles, not on externally mixed dry mineral dust particles.

[59] We find a global mean OH reduction of 10% at the surface and globally when all the heterogeneous reactions are included (Table 12), which leads to an increase of the CO burden by 7%. The whole set of heterogeneous reactions also reduces the NO and NO_2 burdens by 20% and 29%, respectively. HNO_3 is mainly reduced by uptake on mineral dust particles, which leads to a global mean reduction of 15% at the surface and of 22% at 725 hPa while the global burden decreases by 34% (Table 12). *Martin et al.* [2003] found a decrease in OH surface concentration ranging from 5% to 25% over much of the Northern Hemisphere (but this includes also the photochemical effect of aerosols which is not accounted for in our sensitivity simulations NOHETDU and NOHET) which

resulted in an increase in CO surface concentration of 5–10% over much of the Northern Hemisphere.

[60] In our coupled model, the change in oxidant concentrations (i.e., O_3 and OH) affects the sulfur chemistry. For example the DMS burden increases by 11%, as a result of the decrease in OH. SO_2 surface concentrations decrease in average by 14% because of the whole set of heterogeneous reactions with the uptake of SO_2 on sea salt being the major process. When we consider the NOSO4HET simulation (in which the SO_2 uptake on mineral dust and sea salt do not lead to sulfate production), the global mean sulfate concentration at the surface is higher by 26% in the BASE simulation. The impact of trace gas–aerosol interactions on aerosol global distributions and burdens is further presented in part two of this study [*Pozzoli et al.*, 2008].

5. Summary and Conclusions

[61] In this paper we introduced the ECHAM5-HAMMOZ aerosol-chemistry-climate fully coupled model which includes a comprehensive representation of the NOx-Ox-hydrocarbons chemistry, a prognostic representation of the aerosol size distribution, composition, and mixing state as well as the main trace gas–aerosol interactions, such as online calculation of photolysis rates, sulfur chemistry, and heterogeneous reactions. We then applied the model to quantify the effect of the trace gas–aerosol interactions on the global and regional distributions of trace gases. The model evaluation focused on the northwestern Pacific during the TRACE-P experiment, a region which is typically characterized by enhanced aerosol loads. We find that the coupled model reproduces relatively well the general features observed during the TRACE-P experiment, even though there is still room for improvement of the simulations. For example, a mean absolute bias of 20 ppbv (30%) and 40 ppbv (13%) is found for the simulated O_3 and CO concentrations, respectively. Black carbon concentrations are underestimated over the whole tropospheric column, and especially at the surface, by 0.3 μg m^{-3} (mean absolute bias of 80%). This is probably because of too low biomass burning and anthropogenic emissions in southeast Asia and China as suggested by a comparison with the emission inventories of *Carmichael et al.* [2003]. Sulfate concentrations are represented fairly well, especially for latitudes greater than 25°N, while they are overestimated for lower

Table 12. Tropospheric Burdens of Trace Gases for the BASE Simulation and the Ratios With the Sensitivity Simulations NOHETDU, NOHET, and NOSO4HET[a]

	BASE	$\frac{BASE}{NOHETDU}$	$\frac{BASE}{NOHET}$	$\frac{BASE}{NOSO4HET}$
O_3	3.99×10^2	0.98	0.93	1.00
OH	2.09×10^{-4}	0.95	0.91	0.99
NO	5.26×10^{-2}	0.94	0.80	1.00
NO_2	3.16×10^{-1}	0.96	0.71	1.00
HNO_3	1.03	0.70	0.66	1.02
CO	3.66×10^2	1.02	1.07	1.00
SO_2	7.33×10^{-1}	1.01	1.01	1.09
H_2SO_4	6.34×10^{-4}	1.02	1.00	1.06
DMS	5.19×10^{-2}	1.02	1.11	1.01

[a]Unit is Tg. The burdens of SO_2, H_2SO_4, and DMS are expressed in Tg(S).

latitudes (mean absolute bias of 110%). The size distribution, number concentration, surface area, and optical properties tend to be reproduced fairly well by the coupled model although the agreement is generally better near the surface where the aerosol loading is higher than in the upper troposphere where the model consistently underestimates these quantities. This supports the hypothesis of a missing upper tropospheric aerosol source, such as SOAs, or a too large scavenging rate.

[62] We find that heterogeneous reactions decrease O_3 by $18-23\%$ near the surface. Only a small reduction $(2-3\%)$ is due to reactions on mineral dust (and especially in the region north of $25°N$ where the mineral dust loading is larger).

[63] We find that heterogeneous reactions result in a 7% reduction of the global annual mean O_3 burden and in a maximal 15% reduction of the surface O_3 concentration in mineral dust source region (Sahara and its outflow region). Heterogeneous reactions on mineral dust contribute only to a decrease of the global O_3 burden by 2%. Accounting for the heterogeneous reactions leads to a reduction in global mean OH of up to 10% at surface and a corresponding increase in the CO burden of 7%. SO_2 is influenced by uptake on sea salt and mineral dust, and by the changes in oxidant concentrations (such as O_3 and OH that are involved in the sulfur chemistry cycle), with a maximum reduction of 12% in the middle troposphere.

[64] As a consequence, and similarly to previous studies, we conclude that heterogeneous chemistry significantly influences the regional and global distributions of a number of key trace gases (and also of aerosols as discussed by *Pozzoli et al.* [2008]). We suggest however that the choice of uptake coefficients for a given species appears to be the critical parameter that determines the global impact of heterogeneous chemistry on a trace gas (rather than the description of aerosol properties and distributions) as indicated by a comparison of our results to those from previous studies. For example, using uptake coefficients of N_2O_5 on various type of aerosols as recommended by *Evans and Jacob* [2005], we find an annual and global average uptake coefficient (on all aerosols) of 0.023 for N_2O_5, which is similar to the value of *Evans and Jacob* [2005], even though a very different description of the aerosol states is used in their global model (e.g., a bulk approach in that particular case). A prognostic description of size distribution and mixing state of aerosols is important, however, to account for the effect of heterogeneous chemistry on aerosols and thus determine their composition, optical properties, and lifetime as further discussed by *Pozzoli et al.* [2008].

[65] Our current model representation of trace gas–aerosol interactions is limited by a poor knowledge of heterogeneous reactions occurring on internally mixed particles. For example, a better representation of the surface occupied by a single aerosol compound in internally mixed particles is required in order to quantify correctly the uptake of the trace gases on the different aerosol compounds with a specific uptake coefficient. The processes that influence the uptake of trace gases, such as the alkalinity of the mineral dust particles, the coating by sulfate, the possible saturation of the aerosol surface, and the change in solubility of externally mixed particles should be also considered more accurately.

References

Alexander, B., R. J. Park, D. J. Jacob, Q. B. Li, R. M. Yantosca, J. Savarino, C. C. W. Lee, and M. H. Thiemens (2005), Sulfate formation in sea-salt aerosols: Constraints from oxygen isotopes, *J. Geophys. Res.*, *110*, D10307, doi:10.1029/2004JD005659.

Allen, D., K. Pickering, and M. Fox-Rabinovitz (2004), Evaluation of pollutant outflow and CO sources during TRACE-P using model-calculated, aircraft-based, and Measurements of Pollution in the Troposphere (MOPITT)-derived CO concentrations, *J. Geophys. Res.*, *109*, D15S03, doi:10.1029/2003JD004250.

Andres, R., and A. Kasgnoc (1998), A time-averaged inventory of subaerial volcanic sulfur emissions, *J. Geophys. Res.*, *103*(D19), 25,251–25,261.

Atkinson, R., L. Baulch, R. Cox, J. Crowley, R. F. Hamson, M. Jenkin, J. Kerr, M. Rossi, and J. Troe (2004), Summary of evaluated kinetic and photochemical data for atmospheric chemistry, technical report, Cambridge Univ., Cambridge, U. K. (Available at http://www.iupac-kinetic.ch.cam.ac.uk/summary/IUPACsumm_web_latest.pdf)

Auvray, M., I. Bey, E. Llull, M. G. Schultz, and S. Rast (2007), A model investigation of tropospheric ozone chemical tendencies in long-range transported pollution plumes, *J. Geophys. Res.*, *112*, D05304, doi:10.1029/2006JD007137.

Bauer, S. E., and D. Koch (2005), Impact of heterogeneous sulfate formation at mineral dust surfaces on aerosol loads and radiative forcing in the Goddard Institute for Space Studies general circulation model, *J. Geophys. Res.*, *110*, D17202, doi:10.1029/2005JD005870.

Bauer, S. E., Y. Balkanski, M. Schulz, D. A. Hauglustaine, and F. Dentener (2004), Global modeling of heterogeneous chemistry on mineral aerosol surfaces: Influence on tropospheric ozone chemistry and comparison to observations, *J. Geophys. Res.*, *109*, D02304, doi:10.1029/2003JD003868.

Bell, N., D. Koch, and D. T. Shindell (2005), Impacts of chemistry-aerosol coupling on tropospheric ozone and sulfate simulations in a general circulation model, *J. Geophys. Res.*, *110*, D14305, doi:10.1029/2004JD005538.

Bian, H., and M. Prather (2002), Fast-J2: Accurate simulation of stratospheric photolysis in global chemical models, *J. Atmos. Chem.*, *41*(3), 281–296.

Bian, H., and C. S. Zender (2003), Mineral dust and global tropospheric chemistry: Relative roles of photolysis and heterogeneous uptake, *J. Geophys. Res.*, *108*(D21), 4672, doi:10.1029/2002JD003143.

Briegleb, B. (1992), Delta-Eddington approximation for solar-radiation in the NCAR Community Climate Model, *J. Geophys. Res.*, *97*(D7), 7603–7612.

Carmichael, G. R., et al. (2003), Evaluating regional emission estimates using the TRACE-P observations, *J. Geophys. Res.*, *108*(D21), 8810, doi:10.1029/2002JD003116.

Chameides, W., and A. Stelson (1992), Aqueous-phase chemical processes in deliquescent sea-salt aerosols: A mechanism that couples the atmospheric cycles of S and sea salt, *J. Geophys. Res.*, *97*(D18), 20,565–20,580.

Chapman, S., and T. Cowling (1970), *The Mathematical Theory of Nonuniform Gases*, Cambridge Univ. Press, New York.

Clarke, A. D., et al. (2004), Size distributions and mixtures of dust and black carbon aerosol in Asian outflow: Physiochemistry and optical properties, *J. Geophys. Res.*, *109*, D15S09, doi:10.1029/2003JD004378.

Cofala, J., M. Amann, and R. Mechler (2005), Scenarios of world anthropogenic emissions of air pollutants and methane up to 2030, technical report, Int. Inst. for Appl. Syst. Anal., Laxenburg, Austria. (Available at http://www.iiasa.ac.at/rains/global_emiss/global_emiss.html)

Croft, B., U. Lohmann, and K. von Salzen (2005), Black carbon ageing in the Canadian Centre for Climate Modelling and Analysis Atmospheric General Circulation Model, *Atmos. Chem. Phys.*, *5*, 1931–1949.

Davis, E. (1983), Transport phenomena with single aerosol-particles, *Aerosol Sci. Technol.*, *2*(2), 121–144.

Dentener, F., G. Carmichael, Y. Zhang, J. Lelieveld, and P. Crutzen (1996), Role of mineral aerosol as a reactive surface in the global troposphere, *J. Geophys. Res.*, *101*(D17), 22,869–22,889.

Dentener, F., et al. (2006), Emissions of primary aerosol and precursor gases in the years 2000 and 1750, prescribed data-sets for AEROCOM, *Atmos. Chem. Phys. Disc.*, *6*, 2703–2763.

Ebert, E., and J. Curry (1992), A parameterization of ice-cloud optical properties for climate models, *J. Geophys. Res.*, *97*(D4), 3831–3836.

Eisele, F. L., et al. (2003), Summary of measurement intercomparisons during TRACE-P, *J. Geophys. Res.*, *108*(D20), 8791, doi:10.1029/2002JD003167.

Evans, M. J., and D. J. Jacob (2005), Impact of new laboratory studies of N_2O_5 hydrolysis on global model budgets of tropospheric nitrogen oxides, ozone, and OH, *Geophys. Res. Lett.*, *32*, L09813, doi:10.1029/2005GL022469.

Feichter, J., E. Kjellstrom, H. Rodhe, F. Dentener, J. Lelieveld, and G. Roelofs (1996), Simulation of the tropospheric sulfur cycle in a global climate model, *Atmos. Environ.*, *30*(10–11), 1693–1707.

Feng, Y., J. E. Penner, S. Sillman, and X. Liu (2004), Effects of cloud overlap in photochemical models, *J. Geophys. Res.*, *109*, D04310, doi:10.1029/2003JD004040.

Fiore, A. M., L. W. Horowitz, D. W. Purves, H. Levy II, M. J. Evans, Y. Wang, Q. Li, and R. M. Yantosca (2005), Evaluating the contribution of changes in isoprene emissions to surface ozone trends over the eastern United States, *J. Geophys. Res.*, *110*, D12303, doi:10.1029/2004JD005485.

Fouquart, Y., and B. Bonnel (1980), Computation of solar heating of the earth's atmosphere: A new parameterization, *Beitr. Phys. Atmos.*, *53*, 35–62.

Ganzeveld, L., and J. Lelieveld (1995), Dry deposition parameterization in a chemistry general circulation model and its influence on the distribution of reactive trace gases, *J. Geophys. Res.*, *100*(D10), 20,999–21,012.

Ganzeveld, L., J. Lelieveld, and G. Roelofs (1998), A dry deposition parameterization for sulfur oxides in a chemistry and general circulation model, *J. Geophys. Res.*, *103*(D5), 5679–5694.

Ganzeveld, L., J. van Aardenne, T. Butler, M. Lawrence, S. Metzger, P. Zimmermann, and J. Lelieveld (2006), Technical note: Anthropogenic and natural offline emissions and the online Emissions and Dry Deposition submodel EMDEP of the Modular Earth Submodel System (MESSy), *Atmos. Chem. Phys. Disc.*, *6*, 5457–5483.

Grewe, V., D. Brunner, M. Dameris, J. L. Grenfell, R. Hein, D. Shindell, and J. Staehelin (2001), Origin and variability of upper tropospheric nitrogen oxides and ozone at northern mid-latitudes, *Atmos. Environ.*, *35*(20), 3421–3433.

Grewe, V., M. Dameris, C. Fichter, and D. Lee (2002), Impact of aircraft NOx emissions. part 2: Effects of lowering the flight altitude, *Meteorol. Z.*, *11*(3), 197–205.

Guenther, A., et al. (1995), A global-model of natural volatile organic-compound emissions, *J. Geophys. Res.*, *100*(D5), 8873–8892.

Guenther, A., T. Karl, P. Harley, C. Wiedinmyer, P. Palmer, and C. Geron (2006), Estimates of global terrestrial isoprene emissions using MEGAN (Model of Emissions of Gases and Aerosols from Nature), *Atmos. Chem. Phys.*, *6*, 3181–3210.

Hallquist, M., D. Stewart, S. Stephenson, and R. Cox (2003), Hydrolysis of N_2O_5 on sub-micron sulfate aerosols, *Phys. Chem. Chem. Phys.*, *5*(16), 3453–3463.

Halmer, M., H. Schmincke, and H. Graf (2002), The annual volcanic gas input into the atmosphere, in particular into the stratosphere: A global data set for the past 100 years, *J. Volcanol. Geotherm. Res.*, *115*(3–4), 511–528.

Hanisch, F., and J. Crowley (2001), The heterogeneous reactivity of gaseous nitric acid on authentic mineral dust samples, and on individual mineral and clay mineral components, *Phys. Chem. Chem. Phys.*, *3*(12), 2474–2482.

Heald, C. L., et al. (2003), Asian outflow and trans-Pacific transport of carbon monoxide and ozone pollution: An integrated satellite, aircraft, and model perspective, *J. Geophys. Res.*, *108*(D24), 4804, doi:10.1029/2003JD003507.

Heald, C. L., D. J. Jacob, R. J. Park, L. M. Russell, B. J. Huebert, J. H. Seinfeld, H. Liao, and R. J. Weber (2005), A large organic aerosol source in the free troposphere missing from current models, *Geophys. Res. Lett.*, *32*, L18809, doi:10.1029/2005GL023831.

Hoppel, W. A., and P. F. Caffrey (2005), Oxidation of S(IV) in sea-salt aerosol at high pH: Ozone versus aerobic reaction, *J. Geophys. Res.*, *110*, D23202, doi:10.1029/2005JD006239.

Horowitz, L. W., et al. (2003), A global simulation of tropospheric ozone and related tracers: Description and evaluation of MOZART, version 2, *J. Geophys. Res.*, *108*(D24), 4784, doi:10.1029/2002JD002853.

Huebert, B. J., T. Bates, P. B. Russell, G. Shi, Y. J. Kim, K. Kawamura, G. Carmichael, and T. Nakajima (2003), An overview of ACE-Asia: Strategies for quantifying the relationships between Asian aerosols and their climatic impacts, *J. Geophys. Res.*, *108*(D23), 8633, doi:10.1029/2003JD003550.

Jacob, D. (2000), Heterogeneous chemistry and tropospheric ozone, *Atmos. Environ.*, *34*(12–14), 2131–2159.

Jacob, D. J., J. H. Crawford, M. M. Kleb, V. S. Connors, R. J. Bendura, J. L. Raper, G. W. Sachse, J. C. Gille, L. Emmons, and C. L. Heald (2003), Transport and Chemical Evolution over the Pacific (TRACE-P) aircraft mission: Design, execution, and first results, *J. Geophys. Res.*, *108*(D20), 9000, doi:10.1029/2002JD003276.

Jeuken, A., P. Siegmund, L. Heijboer, J. Feichter, and L. Bengtsson (1996), On the potential of assimilating meteorological analyses in a global climate model for the purpose of model validation, *J. Geophys. Res.*, *101*(D12), 16,939–16,950.

Jordan, C. E., J. E. Dibb, B. E. Anderson, and H. E. Fuelberg (2003), Uptake of nitrate and sulfate on dust aerosols during TRACE-P, *J. Geophys. Res.*, *108*(D21), 8817, doi:10.1029/2002JD003101.

Kanakidou, M., et al. (2005), Organic aerosol and global climate modelling: A review, *Atmos. Chem. Phys.*, *5*, 1053–1123.

Kane, S., F. Caloz, and M. Leu (2001), Heterogeneous uptake of gaseous N_2O_5 by $(NH4)(2)SO_4$, NH_4HSO_4, and H_2SO_4 aerosols, *J. Phys. Chem. A*, *105*(26), 6465–6470.

Karagulian, F., and M. Rossi (2005), The heterogeneous chemical kinetics of NO_3 on atmospheric mineral dust surrogates, *Phys. Chem. Chem. Phys.*, *7*(17), 3150–3162.

Kettle, A., and M. Andreae (2000), Flux of dimethylsulfide from the oceans: A comparison of updated data seas and flux models, *J. Geophys. Res.*, *105*(D22), 26,793–26,808.

Kinnison, D. E., et al. (2007), Sensitivity of chemical tracers to meteorological parameters in the MOZART-3 chemical transport model, *J. Geophys. Res.*, *112*, D20302, doi:10.1029/2006JD007879.

Koch, D. (2001), Transport and direct radiative forcing of carbonaceous and sulfate aerosols in the GISS GCM, *J. Geophys. Res.*, *106*(D17), 20,311–20,332.

Liao, H., and J. H. Seinfeld (2005), Global impacts of gas-phase chemistry-aerosol interactions on direct radiative forcing by anthropogenic aerosols and ozone, *J. Geophys. Res.*, *110*, D18208, doi:10.1029/2005JD005907.

Liao, H., P. J. Adams, S. H. Chung, J. H. Seinfeld, L. J. Mickley, and D. J. Jacob (2003), Interactions between tropospheric chemistry and aerosols in a unified general circulation model, *J. Geophys. Res.*, *108*(D1), 4001, doi:10.1029/2001JD001260.

Liao, H., J. H. Seinfeld, P. J. Adams, and L. J. Mickley (2004), Global radiative forcing of coupled tropospheric ozone and aerosols in a unified general circulation model, *J. Geophys. Res.*, *109*, D16207, doi:10.1029/2003JD004456. (Correction, *J. Geophys. Res.*, 109, D24204, doi:10.1029/2004JD005476, 2004.)

Lin, S., and R. Rood (1996), Multidimensional flux-form semi-Lagrangian transport schemes, *Mon. Weather Rev.*, *124*(9), 2046–2070.

Logan, J. (1999), An analysis of ozonesonde data for the troposphere: Recommendations for testing 3-D models and development of a gridded climatology for tropospheric ozone, *J. Geophys. Res.*, *104*(D13), 16,115–16,149.

Lohmann, U., and E. Roeckner (1996), Design and performance of a new cloud microphysics scheme developed for the ECHAM general circulation model, *Clim. Dyn.*, *12*(8), 557–572.

Maahs, H. (1983), Kinetics and mechanism of the oxidation of S(IV) by ozone in aqueous-solution with particular reference to SO_2 conversion in nonurban tropospheric clouds, *J. Geophys. Res.*, *88*, 721–732.

Martin, L., D. Damschen, and H. Judeikis (1981), The reactions of nitrogen-oxides with SO_2 in aqueous aerosols, *Atmos. Environ.*, *15*(2), 191–195.

Martin, R., D. Jacob, R. Yantosca, M. Chin, and P. Ginoux (2003), Global and regional decreases in tropospheric oxidants from photochemical effects of aerosols, *J. Geophys. Res.*, *108*(D3), 4097, doi:10.1029/2002JD002622.

Mayol-Bracero, O. L., P. Guyon, B. Graham, G. Roberts, M. O. Andreae, S. Decesari, M. C. Facchini, S. Fuzzi, and P. Artaxo (2002), Water-soluble organic compounds in biomass burning aerosols over Amazonia: 2. Apportionment of the chemical composition and importance of the polyacidic fraction, *J. Geophys. Res.*, *107*(D20), 8091, doi:10.1029/2001JD000522.

Mishchenko, M., J. Dlugach, E. Yanovitskij, and N. Zakharova (1999), Bidirectional reflectance of flat, optically thick particulate layers: An efficient radiative transfer solution and applications to snow and soil surfaces, *J. Quant. Spectrosc. Radiat. Transfer*, *63*(2–6), 409–432.

Mlawer, E., S. Taubman, P. Brown, M. Iacono, and S. Clough (1997), Radiative transfer for inhomogeneous atmospheres: RRTM, a validated correlated-k model for the longwave, *J. Geophys. Res.*, *102*(D14), 16,663–16,682.

Morcrette, J., S. Clough, E. Mlawer, and M. Iacono (1998), Impact of a validated radiative transfer scheme, RRTM, on the ECMWF model climate and 10-day forecasts, *Tech. Rep. 252*, Eur. Cent. for Med.-Range Weather Forecasts, Reading, U. K.

Nightingale, P., G. Malin, C. Law, A. Watson, P. Liss, M. Liddicoat, J. Boutin, and R. Upstill-Goddard (2000), In situ evaluation of air-sea gas exchange parameterizations using novel conservative and volatile tracers, *Global Biogeochem. Cycles*, *14*(1), 373–387.

Nordeng, T. (1994), Extended versions of the convective parameterization scheme at ECMWF and their impact on the mean and transient activity of the model in the tropics, *Tech. Rep. 206*, Eur. Cent. for Med.-Range Weather Forecasts, Reading, U. K.

Pham, M., J. Muller, G. Brasseur, C. Granier, and G. Megie (1995), A three-dimensional study of the tropospheric sulfur cycle, *J. Geophys. Res.*, *100*(D12), 26,061–26,092.

Pozzoli, L. (2007), Climate and chemistry interactions: Develpment and evaluation of a coupled chemistry-aerosol-climate model, Ph.D. thesis, Ecole Polytech. Fed. de Lausanne, Lausanne, Switzerland.

Pozzoli, L., I. Bey, J. Rast, M. Schultz, P. Stier, and J. Feichter (2008), Trace gas and aerosol interactions in the fully coupled model of aerosol-chemistry-climate ECHAM5-HAMMOZ: 2. Impact of heterogeneous chemistry on the global aerosol distributions, *J. Geophys. Res.*, doi:10.1029/2007JD009008, in press.

Randel, W., F. Wu, J. Russell, A. Roche, and J. Waters (1998), Seasonal cycles and QBO variations in stratospheric CH_4 and H_2O observed in UARS HALOE data, *J. Atmos. Sci.*, *55*(2), 163–185.

Ravishankara, A. (1997), Heterogeneous and multiphase chemistry in the troposphere, *Science*, *276*(5315), 1058–1065.

Ravishankara, A., et al. (2004), Climate chemistry interactions. A report from the joint SPARC/IGAC Workshop, *IGACtivities Newsl.*, *30*, 2–20.

Riemer, N., H. Vogel, and B. Vogel (2004), Soot aging time scales in polluted regions during day and night, *Atmos. Chem. Phys.*, *4*, 1885–1893.

Rockel, B., E. Raschke, and B. Weyres (1991), A parameterization of broad band radiative transfer properties of water, ice and mixed clouds, *Beitr. Phys. Atmos.*, *64*, 1–12.

Roeckner, E., et al. (2003), The atmospheric general circulation model ECHAM5: Part 1, *Tech. Rep. 349*, Max Planck Inst. for Meteorol., Hamburg, Germany.

Rudich, Y., R. Talukdar, and A. Ravishankara (1996), Reactive uptake of NO_3 on pure water and ionic solutions, *J. Geophys. Res.*, *101*(D15), 21,023–21,031.

Sander, S., et al. (2003), Chemical kinetics and photochemical data for use in atmospheric studies, evaluation number 14, *JPL Publ. 02-25*, Jet Propul. Lab., Calif. Inst. of Technol., Pasadena. (Available at http://jpldataeval.jpl.nasa.gov/pdf/JPL_02-25_rev02.pdf)

Schultz, M., A. Heil, J. Hoelzemann, A. Spessa, K. Thonicke, J. Goldammer, A. Held, J. Pereira, and M. van het Bolscher (2008), Global wildland fire emissions from 1960 to 2000, *Global Biogeochem. Cycles*, doi:10.1029/2007GB003031, in press.

Schulz, M., G. de Leeuw, and Y. Balkanski (2004), Sea-salt aerosol source functions and emissions, in *Emissions of Atmospheric Trace Compounds*, pp. 333–359, Springer, New York.

Schwartz, S. (1986), Mass-transport considerations pertinent to aqueous-sphase reactions of gases in liquid-water clouds, in *Chemistry of Multiphase Atmospheric Systems*, pp. 415–471, Springer, New York.

Seinfeld, J., and S. Pandis (1997), *Atmospheric Chemistry and Physics*, John Wiley, New York.

Simmons, A., D. Burridge, M. Jarraud, C. Girard, and W. Wergen (1989), The ECMWF medium-range prediction models development of the numerical formulations and the impact of increased resolution, *Meteorol. Atmos. Phys.*, *40*(1–3), 28–60.

Song, C., and G. Carmichael (2001), A three-dimensional modeling investigation of the evolution processes of dust and sea-salt particles in east Asia, *J. Geophys. Res.*, *106*(D16), 18,131–18,154.

Stevenson, D. S., et al. (2006), Multimodel ensemble simulations of present-day and near-future tropospheric ozone, *J. Geophys. Res.*, *111*, D08301, doi:10.1029/2005JD006338.

Stier, P., et al. (2005), The aerosol-climate model ECHAM5-HAM, *Atmos. Chem. Phys.*, *5*, 1125–1156.

Tang, Y., et al. (2003), Impacts of aerosols and clouds on photolysis frequencies and photochemistry during TRACE-P: 2. Three-dimensional study using a regional chemical transport model, *J. Geophys. Res.*, *108*(D21), 8822, doi:10.1029/2002JD003100.

Tegen, I., S. P. Harrison, K. Kohfeld, I. C. Prentice, M. Coe, and M. Heimann (2002), Impact of vegetation and preferential source areas on global dust aerosol: Results from a model study, *J. Geophys. Res.*, *107*(D21), 4576, doi:10.1029/2001JD000963.

Thomas, K., A. Volz-Thomas, D. Mihelcic, H. Smit, and D. Kley (1998), On the exchange of NO_3 radicals with aqueous solutions: Solubility and sticking coefficient, *J. Atmos. Chem.*, *29*(1), 17–43.

Thornton, J., C. Braban, and J. Abbatt (2003), N_2O_5 hydrolysis on sub-micron organic aerosols: The effect of relative humidity, particle phase, and particle size, *Phys. Chem. Chem. Phys.*, *5*(20), 4593–4603.

Tie, X., S. Madronich, S. Walters, D. P. Edwards, P. Ginoux, N. Mahowald, R. Zhang, C. Lou, and G. Brasseur (2005), Assessment of the global impact of aerosols on tropospheric oxidants, *J. Geophys. Res.*, *110*, D03204, doi:10.1029/2004JD005359.

Tiedtke, M. (1989), A comprehensive mass flux scheme for cumulus parameterization in large-scale models, *Mon. Weather Rev.*, *117*(8), 1779–1800.

Tompkins, A. (2002), A prognostic parameterization for the subgrid-scale variability of water vapor and clouds in large-scale models and its use to diagnose cloud cover, *J. Atmos. Sci.*, *59*(12), 1917–1942.

Toon, O., and T. Ackerman (1981), Algorithms for the calculation of scattering by stratified spheres, *Appl. Opt.*, *20*(20), 3657–3660.

Ullerstam, M., R. Vogt, S. Langer, and E. Ljungstrom (2002), The kinetics and mechanism of SO_2 oxidation by O-3 on mineral dust, *Phys. Chem. Chem. Phys.*, *4*(19), 4694–4699.

Ullerstam, M., M. Johnson, R. Vogt, and E. Ljungstrom (2003), Drifts and Knudsen cell study of the heterogeneous reactivity of SO_2 and NO_2 on mineral dust, *Atmos. Chem. Phys.*, *3*, 2043–2051.

Usher, C. R., H. Al-Hosney, S. Carlos-Cuellar, and V. H. Grassian (2002), A laboratory study of the heterogeneous uptake and oxidation of sulfur dioxide on mineral dust particles, *J. Geophys. Res.*, *107*(D23), 4713, doi:10.1029/2002JD002051.

Usher, C., A. Michel, and V. Grassian (2003), Reactions on mineral dust, *Chem. Rev.*, *103*(12), 4883–4939.

van der Werf, G., J. Randerson, G. Collatz, and L. Giglio (2003), Carbon emissions from fires in tropical and subtropical ecosystems, *Global Change Biol.*, *9*(4), 547–562.

Vignati, E., J. Wilson, and P. Stier (2004), M7: An efficient size-resolved aerosol microphysics module for large-scale aerosol transport models, *J. Geophys. Res.*, *109*, D22202, doi:10.1029/2003JD004485.

Wild, O., X. Zhu, and M. Prather (2000), Fast-J: Accurate simulation of in- and below-cloud photolysis in tropospheric chemical models, *J. Atmos. Chem.*, *37*(3), 245–282.

World Meteorological Organization (1992), *International Meteorological Vocabulary*, 2nd ed., 784 pp., Geneva, Switzerland.

Zhang, Y., and G. Carmichael (1999), The role of mineral aerosol in tropospheric chemistry in east Asia—A model study, *J. Appl. Meteorol.*, *38*(3), 353–366.

————————————

I. Bey, Laboratoire de Modélisation de la Chimie Atmosphérique, École Polytechnique Fédérale de Lausanne, Station 2, Lausanne CH-1015, Switzerland.

J. Feichter, L. Pozzoli, and S. Rast, Atmosphere in Earth System, Max Planck Institute for Meteorology, Hamburg D-20146, Germany. (luca.pozzoli@epfl.ch)

M. G. Schultz, Institute of Chemistry and Dynamics of the Geosphere: Troposphere, Forschungzentrum, Jülich D-52425, Germany.

P. Stier, Atmospheric, Oceanic and Planetary Physics, University of Oxford, Oxford OX1 3PU, UK.